N_2O rate of change as a diagnostic of the Brewer-Dobson Circulation in the stratosphere

Daniele Minganti [1], Simon Chabrillat [1], Quentin Errera [1], Maxime Prignon [2*], Douglas E. Kinnison [3], Rolando R. Garcia [3], Marta Abalos[4], Justin Alsing[5,9], Matthias Schneider [6], Dan Smale [7], Nicholas Jones [8], Emmanuel Mahieu [2]

[1]Royal Belgian Institute for Space Aeronomy, BIRA-IASB, Brussels, Belgium
[2]Institute of Astrophysics and Geophysics, UR SPHERES, University of Liège, Liège, Belgium
[3]National Center for Atmospheric Research, Boulder, CO, USA
[4]Universidad Complutense de Madrid, Madrid, Spain
[5]Oskar Klein Centre for Cosmoparticle Physics, Department of Physics, Stockholm University, Stockholm SE-106 91, Sweden
[6]Karlsruhe Institute of Technology, Karlsruhe, Germany
[7]National Institute of Water and Atmospheric Research, Lauder, New Zealand
[8]School of Chemistry, University of Wollongong, Wollongong, Australia
[9]Imperial Centre for Inference and Cosmology, Department of Physics, Imperial College London, Blackett Laboratory, Prince Consort Road, London SW7 2AZ, UK

Key Points:

- The poor sampling of the Atmospheric Chemistry Experiment Fourier Transform Spectrometer exaggerates the stratospheric nitrous oxide trends
- Decadal trends of nitrous oxide are less significant in the northern extratropics due to a larger short-timescale variability of transport
- The Transformed Eulerian Mean analysis shows that the residual advection contributes to the positive nitrous oxide trends over the Tropics

*Currently at: Department of Earth, Space and Environment, Chalmers University of Technology, 41296, Gothenburg, Sweden

Corresponding author: Daniele Minganti, `daniele.minganti@aeronomie.be`

Abstract

The Brewer-Dobson Circulation (BDC) determines the distribution of long-lived tracers in the stratosphere; therefore, their changes can be used to diagnose changes in the BDC. We investigate decadal (2005-2018) trends of nitrous oxide (N_2O) stratospheric columns (12-40 km) as measured by four Fourier transform infrared (FTIR) ground-based instruments and by the Atmospheric Chemistry Experiment Fourier Transform Spectrometer (ACE-FTS), and compare them with simulations by two models: a chemistry-transport model (CTM) driven by four different reanalyses, and the Whole Atmosphere Chemistry-Climate Model (WACCM). The limited sensitivity of the FTIR instruments can hide negative N_2O trends in the mid-stratosphere because of the large increase in the lowermost stratosphere. When applying the ACE-FTS sampling on model datasets, the reanalyses by the European Centre for Medium Range Weather Forecast (ECMWF) compare best with ACE-FTS, but the N_2O trends are consistently exaggerated. Model sensitivity tests show that while decadal N_2O trends reflect changes in transport, these trends are less significant in the northern extratropics due to the larger variability of transport over timescales shorter than two years in that region. We further investigate the N_2O Transformed Eulerian Mean (TEM) budget in three model datasets. The TEM analysis shows that enhanced advection affects the stratospheric N_2O trends more than changes in mixing. While no ideal observational dataset currently exists, this model study of N_2O trends still provides new insights about the BDC and its changes thanks to relevant sensitivity tests and the TEM analysis.

Plain Language Summary

The circulation in the stratosphere is characterized by upward motion above the Tropics, followed by poleward and downward motions above the high latitudes. Changes in the pattern of this stratospheric circulation are currently a challenging topic of research. We investigate the decennial changes of this stratospheric circulation using observations and numerical simulations of the long-lived tracer nitrous oxide. Observations are obtained from ground-based and satellite instruments. Numerical simulations include complex atmospheric models that reproduce the chemistry and dynamics of the stratosphere. Both observations and models show differences between the hemispheres in the nitrous oxide decennial changes. Unfortunately, the current observations of nitrous oxide are not perfect. The ground-based instruments cannot correctly measure the changes of nitrous oxide in the northern hemisphere. The satellite does not measure at all times, and it spatially covers more the high latitudes, which negatively affects the measurements of nitrous oxide. On the other side, model simulations can provide valuable insights into the changes in the stratospheric circulation. They show that changes in the stratospheric circulation cause the differences between hemispheres in the nitrous oxide tendencies. In addition, the model simulations show that the circulation changes can be associated with different physical contributions.

1 Introduction

Nitrous oxide (N_2O) is continuously emitted in the troposphere, with a nearly constant rate of change of 2% per decade, and transported into the stratosphere, where it is destroyed by photodissociation mainly in the Tropics (Tian et al., 2020). The atmospheric lifetime of N_2O is approximately 120 years, which makes it an excellent tracer for stratospheric transport studies (Seinfeld & Pandis, 2016). Changes in ozone abundances have been studied and attributed to chemical and dynamical contributions (Petropavlovskikh et al., 2019). Recently, Ball et al. (2018) discussed positive ozone trends in the lower stratosphere and attributed them to changes in transport. However, the ozone distribution in the middle and upper stratosphere is largely impacted by changes in its chemistry. Hence, long-lived tracers as N_2O are more relevant than ozone to investigate transport changes with little interference from the chemistry.

The transport in the stratosphere is enabled by the Brewer-Dobson Circulation (BDC), a wave-driven circulation that consists of upwelling in the Tropics followed by poleward transport and downwelling in the extratropics (Plumb, 2002). For tracer transport, the BDC is often separated into an advective component, the residual meridional circulation, and a quasi-horizontal mixing component (Shepherd, 2007). The BDC has a significant impact in determining the stratospheric distribution of chemical tracers, like ozone and greenhouse gases (GHGs), and in the momentum and heat budgets of the stratosphere (e.g., Butchart, 2014).

Long-term changes in the BDC could have significant impacts on the climate system. One of the most important is the effect on the recovery of stratospheric ozone, as a changing BDC would result in changes of the meridional distribution of ozone (e.g., Shepherd, 2008; Dhomse et al., 2018). The lifetime of Ozone Depleting Substances (ODS) in the stratosphere is also impacted by changes in the BDC (Butchart & Scaife, 2001; Waugh & Hall, 2002), as well as the water vapor entering the stratosphere in the Tropics (e.g., W. Randel & Park, 2019). The troposphere is also impacted by the BDC changes in terms of mass exchange with the stratosphere (e.g., ozone, Meul et al., 2018), and of the harmful ultra-violet radiation reaching the surface (Meul et al., 2016).

Understanding the changes in the BDC is thus fundamental to fully comprehend the past and future evolution of climate. Simulations by Chemistry-Climate Models (CCMs) robustly project an acceleration of the BDC throughout the stratosphere in recent and coming decades due to the increase of GHGs (e.g., Hardiman et al., 2014; Abalos et al., 2021). On the other hand, Oberländer-Hayn et al. (2016) argue that the global BDC trends in the lower stratosphere in CCMs are caused by a lift of the tropopause in response to global warming rather than an actual speedup of the circulation. Other modeling studies have shown that mixing also plays an important role in the simulated BDC changes, and is also the primary reason for the differences in the simulated BDC changes among CCMs (e.g., Eichinger et al., 2019). Recent studies have also shown that ODS, through their impact on ozone, play a significant role in the modeled BDC changes, and that ODS decreases resulting from the Montreal Protocol, will reduce the global warming-induced acceleration of the BDC (e.g., Polvani et al., 2019; Abalos et al., 2020).

The BDC can be quantified indirectly from measurements of long-lived tracers or temperature (e.g., Fu et al., 2015; Engel et al., 2009). Recently, Strahan et al. (2020) used ground-based observations of nitric acid and hydrogen chloride to investigate hemispheric-dependent BDC changes in the stratosphere. The Age of Air (AoA) is a widely used diagnostic for stratospheric transport, and is defined as the transit time of an air parcel from the tropical tropopause (or the surface, depending on the definition) to a certain point of the stratosphere (Waugh & Hall, 2002). Engel et al. (2017) used balloon-borne observations of carbon dioxide and methane to derive mean AoA trends above the northern mid-latitudes in the mid-lower stratosphere. They found positive but not statistically significant AoA trends over about 40 years (corresponding to a slowdown of the BDC), which is in contrast with model results that anticipate a significant acceleration of the BDC. These discrepancies can be partly attributed to the temporal and spatial sparseness of the measurements and to uncertainties in the AoA trends derived from real tracers (Garcia et al., 2011; Fritsch et al., 2020).

Satellite measurements of long-lived tracers have been used to compute AoA trends as well (e.g., Stiller et al., 2012; Haenel et al., 2015). These observational studies using remote sensing measurements have shown a hemispheric asymmetry in the AoA trends over the last decade, with positive changes in the Northern Hemisphere (NH) and a negative change in the Southern Hemisphere (SH) (e.g., Mahieu et al., 2014; Stiller et al., 2017; Fu et al., 2019). However, the mean AoA indirectly obtained from satellite measurements does not allow the separation between residual advection and mixing, which was proven to be important in CCMs (Dietmüller et al., 2018). The recent study of von Clarmann and Grabowski (2021) proposes an alternative method to infer the stratospheric circulation from satellite measurements of long-lived tracers by a direct inversion of the continuity equation. When studying BDC trends, it is crucial to consider time scales longer than around 12 years, as the natural variability of the BDC can mask trends computed over shorter periods (Hardiman et al., 2017).

Reanalysis datasets try to fill the gap between observations and free-running models, providing a global multi-decadal and consistent state of the past atmosphere by assimilating available observations. Dynamical fields from reanalyses can be used to drive Chemistry-Transport Models (CTMs) to simulate the distribution of real and synthetic tracers in the atmosphere. In the past decade, these CTMs experiments have been used to investigate BDC changes in reanalyses, providing similar results as the satellite measurements for decadal time scales, as first shown by Monge-Sanz et al. (2013). However, recent studies have shown significant differences in BDC changes obtained from different reanalyses, especially over decadal time scales (e.g., Chabrillat et al., 2018). Furthermore, the computation of AoA largely depends on whether the velocities or the heating rates are used to drive the CTMs, leading to significant differences within the same reanalysis (Ploeger et al., 2019).

Minganti et al. (2020, hereafter M2020) investigated the climatology of stratospheric N_2O and its Transformed Eulerian Mean (TEM) budget in a CCM and in a CTM driven by dynamical reanalyses. The TEM diagnostic allows separating the effects of transport and chemistry on the rate of change of a stratospheric tracer such as N_2O (Andrews et al., 1987; W. J. Randel et al., 1994). Within the TEM framework, the impact of transport can be further separated into the impact from the residual mean advection and mixing, as was done for ozone in Abalos et al. (2013). In this study, we aim to investigate multi-decadal and decadal changes of stratospheric N_2O and the impact of the BDC on those changes in both observations and model simulations. We use ground-based observations of N_2O from Fourier transform infrared (FTIR) spectrometers that are part of the Network for the Detection of Atmospheric Composition Change (NDACC) at four stations in the SH and NH subtropics as well as at mid-latitudes (De Mazière et al., 2018, `http://www.ndaccdemo.org/`). We compare these FTIR observations with satellite measurements from the Atmospheric Chemistry Experiment Fourier Transform Spectrometer (ACE-FTS, P. Bernath et al., 2021). Contrary to M2020, who used the chemical reanalysis of N_2O measured by the Aura Microwave Limb Sounder (MLS) within their comparison (Errera et al., 2019), we cannot use such reanalysis because of the drift in the MLS N_2O dataset (Livesey et al., 2021).

We use four modern reanalyses that are part of the SPARC (Stratosphere-troposphere Processes and their Role in Climate) Reanalysis Intercomparison Project (S-RIP, Fujiwara et al., 2017). These reanalyses drive simulations of the Belgian Assimilation System for Chemical ObsErvation Chemistry-Transport Model CTM (BASCOE CTM, Chabrillat et al., 2018). We compare the observations and the BASCOE CTM simulations with the Whole Atmosphere Community Climate Model (WACCM) version 4 (Garcia et al., 2017) and version 6 (Gettelman et al., 2019).

The present study is structured as follows. Section 2 describes the observational and modeling datasets used in this study, as well as the TEM diagnostics and the regression model used to derive linear trends. In Section 3, we use FTIR observations to evaluate the trends in the N_2O stratospheric columns obtained from satellite measurements and models. In Section 4, using ACE-FTS as a reference, we study the global N_2O trends in the stratosphere and focus on the differences in the trend patterns among datasets. In Section 5, we investigate the N_2O TEM budget for two BASCOE simulations and WACCM version 6 in order to separate the impact of the residual advection and mixing on the

N_2O trends. Finally, Section 6 concludes the study with a summary of the principal findings.

2 Data and Methods

This section describes the observational and model data as well as the methods used in this study (see Tables 1 and 2). Throughout the study, we will refer to the CCMs and the BASCOE CTM simulations as "models" to distinguish them from the observations obtained from the FTIR and ACE-FTS. For the sake of brevity, we refer to M2020 for a more detailed description of the dataset (BASCOE CTM, WACCM version 4, and S-RIP reanalyses) and methods (TEM framework) already used there.

Dataset name	Full Name	Reference	Year range	Vertical resolution
WACCM-REFC1	Whole Atmosphere Community Climate Model	Garcia et al. (2017)	1985-2018	L66, 5.96 10^{-6} hPa
WACCM-REFD1	Whole Atmosphere Community Climate Model	Gettelman et al. (2019)	1985-2018	L70, 5.96 10^{-6} hPa
CTM+ERAI	ECMWF Reanalysis Interim	Dee et al. (2011)	1985-2018	L60, 0.1 hPa
CTM+ERA5	ECMWF Reanalysis 5	Hersbach et al. (2020)	1985-2019	L86, 0.01 hPa
CTM+JRA55	Japanese 55-year Reanalysis	Kobayashi et al. (2015)	1985-2018	L60, 0.2 hPa
CTM+MERRA2	Modern-Era Retrospective analysis for Research and Applications	Gelaro et al. (2017)	1985-2018	L72, 0.01 hPa
ACE-FTS	Atmospheric Chemistry Experiment Fourier Transform Spectrometer	P. Bernath et al. (2021)	2005-present	L42, 150 km

Table 1. Overview of the models and satellite measurements used in this study.

Station name	Reference	Location (lat and lon)	Altitude	strato DOFS
Lauder	Zhou et al. (2019)	45.4°S and 169.68°E	370 m	2
Wollongong	Griffith et al. (2012)	34.45°S and 150.88°E	30 m	2
Izãna	García et al. (2021)	28.30°N and 16.48°E	2367 m	1.5
Jungfraujoch	Zander et al. (2008)	46.55°N and 7.98°E	3580 m	1.1

Table 2. Overview of FTIR stations considered in this study.

2.1 Ground-based FTIR Observations

We use ground-based measurements of stratospheric N_2O columns obtained at four stations that are part of NDACC: Lauder (New Zealand, 45°S), Wollongong (Australia, 34°S), Izãna(Spain, 28°N) and Jungfraujoch (Switzerland, 46°N) (Zhou et al., 2019). The FTIR technique allows the acquisition of long-term consistent ensembles of very high-resolution solar absorption spectra under clear-sky conditions. The stations have been chosen at the mid-latitudes and subtropics where the observed BDC changes are the largest (e.g., Engel et al., 2017; Strahan et al., 2020).

At Jungfraujoch, measurements have been obtained from two spectrometers: an instrument developed at the University of Liège (1984-2008), and a Bruker IFS 120HR (early 1990's-present) (Zander et al., 2008; Prignon et al., 2019). In this study, we use the Bruker spectrometer to investigate the most recent period. Ground-based measurements of N_2O profiles at Lauder started in 2001 with a Bruker 120HR spectrometer, replaced in 2018 (with 6 months overlap) by a Bruker 125HR (Strong et al., 2008; Zhou et al., 2019). The Lauder station is particularly relevant as is the only FTIR site of NDACC located in the SH mid-latitudes. The Wollongong station has provided data for the SH subtropics since 1996. Solar spectra were measured with a Bomem instrument until 2007, which was then replaced by a Bruker 125HR (Griffith et al., 2012). N_2O profiles are also measured at the IzãnaObservatory since 1999. This high-altitude station is characterized by excellent conditions for FTIR spectroscopy, with clear sky conditions for most of the year. Observations started using a Bruker 120M spectrometer and continued, since 2005, with a Bruker 125HR (García et al., 2021). The retrieval code for the N_2O profiles is the SFIT-v4 (v0.9.4.4) for the Jungfraujoch, Lauder and Wollongong stations, and PROFITT9 for the Izãnastation (Zhou et al., 2019).

We consider stratospheric N_2O columns between 12 and 40 km because the instruments at all stations are the most sensitive to the measured N_2O profiles over that layer (not shown). The degrees of freedom for signal (DOFS), which quantify the vertical resolution of the measurement (Rodgers, 2000), largely vary among the stations. For N_2O, the stratospheric DOFS between 12 and 40 km of the instruments above the SH are around 2, allowing the separation of two stratospheric layers. On the other hand, the stratospheric DOFS of the instruments above the NH are around 1.5 for Izãna, and 1 for Jungfraujoch, limiting the analysis to one stratospheric layer between 12 and 40 km. Thus, in order to perform a fair comparison, we compute one stratospheric N_2O column between 12 and 40 km for all stations.

2.2 Spaceborne Measurements - ACE-FTS

ACE-FTS, onboard the SCISAT Canadian satellite, was launched in August 2003 on a high inclination (74°) low earth orbit (650 km) and is still in operation in 2021 (P. F. Bernath et al., 2005; P. Bernath, 2017). ACE-FTS instrument measures the infrared absorptions from solar occultations between 2.2 and 13.3 μm with a spectral resolution of 0.02 cm^{-1}. This allows the retrieval of vertically resolved mixing ratio profiles for 44 molecules and 24 isotopologues from each measurement (P. Bernath et al., 2020).

In this study, we use version 4.1 of the ACE-FTS data. It differs from previous versions by significantly better retrievals at low altitudes and led to substantially improved trends compared to earlier version 3.5 (P. Bernath et al., 2021). For N_2O, previous comparisons of v3.6 with independent satellite instruments showed a good agreement below 35 km (within 10%) and larger biases above that level (within 20%, Sheese et al., 2017). In our study, N_2O profiles are filtered for outliers using the method described in Sheese et al. (2017) and are then vertically regridded to a constant pressure vertical grid using a mass-conservative scheme (Bader et al., 2017). When compared to ground-based measurements, ACE-FTS profiles are vertically interpolated to the grid of the FTIR data applying the averaging kernels of the FTIR retrieval as described in Langerock et al. (2015). For trend analysis, profiles are monthly averaged on latitude bins with 5°spacing from pole to pole.

In order to compare trend analysis of model simulations with those obtained by ACE-FTS, model datasets are first re-sampled as ACE-FTS (this is important in particular due to the low sampling of ACE-FTS - only 30 daily profiles due to the solar occultation method). This is done by finding model output adjacent it time to each ACE-FTS profile (BASCOE and WACCM datasets used in this study have, respectively, 6 hourly and daily output) and then by linearly interpolating the model values in time and space at the profile geolocation. The re-sampled model datasets are then monthly averaged as done with ACE-FTS.

2.3 BASCOE CTM and Driving Reanalyses

In this study, we use the BASCOE CTM driven by four dynamical reanalyses: the European Centre for Medium-Range Weather Forecast Interim reanalysis (ERAI, Dee et al., 2011), and its newer version ERA5 (Hersbach et al., 2020), the Modern-Era Retrospective analysis for Research and Applications (MERRA2, Gelaro et al., 2017), and the Japanese 55-year Reanalysis (JRA55, Kobayashi et al., 2015). In the following, we provide a brief overview of the CTM and the ERAI, MERRA2 and JRA55 reanalyses, because those datasets are already described in a number of companion studies (Chabrillat et al., 2018; Prignon et al., 2019, 2021, M2020). On the other hand, we provide a more detailed description of ERA5, as is the newest reanalysis in this study.

The BASCOE CTM is built on a kinematic transport module (that takes in input the surface pressure and the horizontal winds) with a flux-form semi-Lagrangian (FFSL) advection scheme (S.-J. Lin & Rood, 1996). The FFSL scheme is run on a common horizontal grid of 2°x2.5°for all the reanalyses, while the vertical grid depends on the input reanalysis. The chemical scheme explicitly solves for stratospheric chemistry, and includes 65 chemical species and 243 reactions (Prignon et al., 2019). ERAI and JRA55 have 60 levels up to 0.1 hPa, MERRA2 has 72 levels up to 0.01 hPa. The model setup, as well as the boundary conditions, are the ones used in Prignon et al. (2019), M2020 and Prignon et al. (2021). Refer to Chabrillat et al. (2018) for a detailed description of the BASCOE CTM and its driving by the ERAI, JRA55 and MERRA2 reanalyses.

The ERA5 reanalysis is the fifth generation of reanalysis produced by the ECMWF and covers the 1979-present period, with a programmed extension back to 1950 (Hersbach et al., 2020). The horizontal resolution is 31 km, with hourly output frequency, and the vertical grid ranges from the surface to 0.01 hPa with 137 levels and with 300-600 m vertical spacing in the troposphere and stratosphere, which increases to 1-3 km above 30 km. ERA5 suffers from a cold bias in the lower stratosphere from 2000 and 2006. For this reason, a new analysis (ERA5.1) has been produced for that period to correct for that bias (Simmons et al., 2020). In this study, the BASCOE CTM was driven by ERA5.1 for the 2000-2006 period. For computational reasons, the vertical resolution is reduced to 86 levels from the original 137 keeping the original vertical spacing in the stratosphere, and we used 6-hourly (0000, 0600, 1200, 1800 UTC) data. As done for the other reanalyses, the ERA5 data on the fine 31-km grid were truncated at wavenumber 47 to avoid aliasing on the target 2.5°x2°horizontal grid (Chabrillat et al., 2018).

In order to investigate more the contribution of transport for ERA5, we performed two sensitivity tests with the BASCOE CTM driven by that reanalysis. In order to isolate the contribution of transport, the first sensitivity test consisted of a BASCOE CTM experiment where the N_2O does not increase over time. We accomplished that by performing a BASCOE CTM run exactly as the ERA5 simulation but keeping the N_2O volume mixing ratios at the surface fixed to their values at the beginning of the simulation (cst-N_2O run). Variations in the rate of change of N_2O for cst-N_2O are therefore due only to the effect of transport. The other sensitivity test is complementary to cst-N_2O, and consists of an experiment where the transport does not change over time (cst-dyn). In order to include a complete Quasi Biennial Oscillation cycle (QBO, Baldwin et al., 2001), we used the years 2006 and 2007 from ERA5.1 and ERA5, respectively. Those years are unusual (but convenient) because the QBO lasted exactly 24 months (see the zonal wind data at Singapore `https://www.geo.fu-berlin.de/met/ag/strat/produkte/qbo/singapore.dat`). We used the dynamics of the year 2006 to simulate even years and from the year 2007 for odd years. All the N_2O changes simulated by cst-dyn are due to its constant increase at the surface.

2.4 WACCM

In this study, we use two versions of WACCM: version 4 (Marsh et al., 2013) and version 6 (Gettelman et al., 2019). WACCM version 4 (WACCM4) is the atmospheric component of the Community Earth System Model version 1.2.2 (CESM, Hurrell et al., 2013), which has been developed by the U.S. National Center of Atmospheric Research. It is the extended (whole atmosphere) version of the Community Atmosphere Model version 4 (CAM4, Neale et al., 2013). WACCM4 has a longitude-latitude grid of 2.5°x1.9°and 66 vertical levels from the surface to about 140 km altitude, with 1.1-1.75 km vertical spacing in the stratosphere. The physics of WACCM4 is the same as CAM4 and the dynamical core is a finite volume with a horizontal discretization based on a conservative flux-form semi Lagrangian (FFSL) scheme (S.-J. Lin, 2004). WACCM4 is not able to internally generate the QBO; thus, it is nudged towards observations of stratospheric winds (Matthes et al., 2010). In this study, we use the WACCM4 version included within the SPARC (Stratosphere-troposphere Processes And their Role in Climate) Chemistry-Climate Model Intercomparison phase 1 (CCMI-1, Morgenstern et al., 2017). In particular, we use the REFC1 experiments (WACCM-REFC1), which consist of simulations of the recent past (1960-2018) using state-of-the-art historical forcings and observed sea-surface temperatures (Morgenstern et al., 2017). Compared to the default WACCM4 version, WACCM-REFC1 includes important modifications of the treatment of heterogeneous chemistry and of the gravity waves parameterization, which ultimately improve the simulation of ozone above the Southern Hemispheric (Garcia et al., 2017). In this study, we use three realizations of the WACCM-REFC1 configuration for the 1985-2018 period.

Version 6 of WACCM (WACCM6) is the extension to the whole atmosphere of version 6 of CAM that is part of version 2 of CESM (Danabasoglu et al., 2020). The default horizontal resolution of WACCM6 is 0.9°x1.25°latitude-longitude, with 70 levels in the vertical from the ground to around 140 km, with vertical resolution similar to WACCM4. The transition from WACCM4 to WACCM6 involved several changes in the physics and chemistry that are described in Gettelman et al. (2019). WACCM6 is part of the Coupled Model Intercomparison Project Phase 6 (CMIP6, Eyring et al., 2016), and is used in the CCMI-2022 activity (i.e., the successor of CCMI-1, Plummer et al., 2021). Within CCMI-2022, we use the REFD1 WACCM6 experiments (WACCM-REFD1), i.e., a suite of hindcast experiments for the recent past (1960-2018) used to compare with observations. The REFD1 experiments use the databases for historical forcings and observed sea surface temperatures developed for the CMIP6. Although WACCM6 can internally produce the QBO, the REFD1 experiments require a nudged QBO towards observed winds to ensure synchronization with historical variability. In this study, we use one realization of the WACCM-REFD1 experiments for the 1985-2018 period.

2.5 TEM Diagnostics

For stratospheric tracers, the TEM diagnostics (Andrews et al., 1987) allows separating the impact of transport and chemistry on the zonal mean local rate of change of a tracer with mixing ratio χ:

$$\overline{\chi}_t = -v^*\overline{\chi}_y - w^*\overline{\chi}_z + e^{z/H}\nabla\cdot\mathbf{M} + \overline{S} + \overline{\epsilon}, \qquad (1)$$

where χ represents N_2O, $\mathbf{M} = -e^{-z/H}(\overline{v'\chi'} - \overline{v'\theta'}\bar{\chi}_z/\bar{\theta}_z, \overline{w'\chi'} + \overline{v'\theta'}\bar{\chi}_y/\bar{\theta}_z)$ is the eddy flux vector, and (v^*, w^*) are the meridional and vertical components of the residual circulation, respectively. Overbars denote zonal means and prime quantities indicate deviations from it, while subscripts indicate partial derivatives. $H = 7\ km$ is the scale height, and $z \equiv -Hlog_e(p/p_s)$ is the log-pressure altitude, with the surface pressure $p_s = 10^5 Pa$. The S term is the net rate of change due to chemistry, defined as the difference between the production ($\bar{P}$) and loss ($\bar{L}$) rates $\bar{S} = \bar{P} - \bar{L}$. The $\bar{\epsilon}$ contribution represents the residual of the budget, i.e., the difference between the actual rate of change of χ and the sum of the transport and chemistry terms on the right-side hand of Eq. 1.

The transport terms in Eq. 1 can be grouped as follows:

$$\overline{\chi}_t = ADV + MIX + \overline{S} + \overline{\epsilon}, \tag{2}$$

where $ADV = (-v^*\overline{\chi}_y - w^*\overline{\chi}_z)$ and $MIX = e^{z/H}\nabla \cdot \mathbf{M}$ represent the contribution of the residual advection and of the resolved mixing, respectively. We refer to M2020 for a more detailed description of the TEM framework applied to the N_2O mixing ratios in the stratosphere and for a comprehensive discussion of the contribution of each term to the N_2O budget.

2.6 Derivation of Trends with the Dynamical Linear Modelling Tool

In this study, we investigate decadal trends using the Dynamical Linear Modeling (DLM, Alsing, 2019). DLM is based on Bayesian inference and provides a number of possible models to analyze time series. Each model is characterized by some unknown parameters, and the DLM computes the posterior probability distribution of those parameters using a combination of Kalman filtering and Markov chain Monte Carlo method.

For a given atmospheric time-series y_t, a generic DLM model is composed of four components: a linear background trend, a seasonal cycle with 12- and 6-months periods, forcing terms decribed by a number of regressor variables and an auto-regressive component:

$$\begin{aligned} y_t \quad = \quad & \beta_{1,t}z_{1,t} + \beta_{2,t}z_{2,t} ... + \beta_{n,t}z_{n,t} \\ & + \beta^{12}_{1,t}\sin(2\pi t/12) + \beta^{12}_{2,t}\cos(2\pi t/12) \\ & + \beta^{6}_{1,t}\sin(2\pi t/6) + \beta^{6}_{2,t}\cos(2\pi t/6) \\ & + \mu_t \\ & + z^{AR}_t \\ & + \epsilon_t. \end{aligned} \tag{3}$$

In Eq. 3, the terms $\beta_{i,t}z_{i,t}$ represent the contribution to y_t from each of the regressors. The 6- and 12-months seasonal cycles are modeled respectively by $\beta^6_{1,t}\sin(2\pi t/6)+\beta^6_{2,t}\cos(2\pi t/6)$ and $\beta^{12}_{1,t}\sin(2\pi t/12)+\beta^{12}_{2,t}\cos(2\pi t/12)$. The μ_t term denotes the linear fit term, and z^{AR}_t the auto-regressive term, defined similarly to the Cochrane-Orcutt correction (Kyrölä et al., 2013), and ϵ_t is the uncertainty.

Contrarily to a multi-linear regression (MLR) model, the background linear fit μ_t and the amplitudes of the seasonal cycles $\beta^{6,12}_{i,t}$ in DLM can vary with time (i.e., they are non-parametric). Their degrees of time-dependence are the unknown model parameters and are initially set by the user and inferred from the data during the model run. Furthermore, the auto-regressive process in the DLM is computed within the model run together with the other parameters, not as a post-run correction as done in the MLR, and its uncertainties are carefully taken into account within the error propagation. In addition, the standard DLM implementation has time-varying (heteroscedastic) uncertainty distribution, when time-varying uncertainties are available. DLM was recently used to investigate stratospheric ozone trends in observations and models (Ball et al., 2017, 2018). A more detailed description of the DLM models and their implementation can be found in Laine et al. (2014). For a more comprehensive review of time-series analysis using DLM, refer to Durbin and Koopman (2012).

As regressor variables, we used the 30 cm radio flux as a solar proxy (de Wit et al., 2014), an index for the El-Nino Southern Oscillation (Wolter & Timlin, 2011) from the National Oceanic and Atmospheric Administration (`http://www.esrl.noaa.gov/psd/`

`enso/mei/`), and two indices for the QBO at 30 and 50 hPa from the Freie Universität Berlin (`http://www.geo.fu-berlin.de/en/met/ag/strat/produkte/qbo/index.html`). We fed the DLM model with monthly data, running 3000 samples where the first 1000 were considered as a warmup and discarded. We also tried 10000 realizations and 3000 as warmup with very similar results (not shown). We performed several sensitivity tests to determine the appropriate values of the initial model parameters, i.e., the degree of time-dependence of the linear trend and seasonal cycles, in order to allow a reasonable time-dependence without being unrealistic. The different combinations of these values did not provide significant differences, so we kept the recommended values.

The linear trends are computed from the distribution of the fit samples as the difference of the model realizations between the end and start dates of the period considered (delta), weighted by the number of the years considered. The uncertainties associated with the trend are computed as the percentage of the delta values that are positive (negative). This percentage can be interpreted as the posterior probability that the overall change in the fit is positive (negative) between the considered dates. In this way, we do not make any assumption on the shape of the distribution of the trends. In this study, we show three values of the posterior probability, 80, 90 and 95 %.

3 Stratospheric N_2O Columns and their Trends

Figure 1 shows the monthly linear fits of the N_2O stratospheric columns (12-40 km) at the four FTIR stations, together with the initial N_2O columns for the observations and the ERA5 simulation. In this analysis, we do not apply the FTIR time sampling to the model outputs, because sensitivity tests using the WACCM-REFD1 outputs at each station showed no significant impact of the FTIR time sampling on the recovered trends of the N_2O columns (not shown). The stratospheric N_2O columns computed between 12 and 40 km of altitude are highly sensitive to the N_2O increase in the lower stratosphere, which is the result of the continuous growth in the troposphere (Tian et al., 2020; P. Bernath et al., 2020). Consequently, all datasets exhibit an increase in the stratospheric N_2O columns over the last two decades.

Above Lauder, the linear fit of the stratospheric N_2O columns from the ERA5 simulation is in agreement with the observations, similarly to JRA55 and ERAI. WACCM-REFD1 underestimates the N_2O stratospheric columns compared to the observations by around 10%, and performs worse than its earlier version WACCM-REFC1. At Wollongong, the slope of the linear fit of the N_2O columns measured by the FTIR, and to a lesser extent by ACE-FTS, is steeper before 2005 compared to the following period. This change of gradient is not visible in any of the model simulations. On the contrary, some of the models show a slower increase before 2005, followed by a more rapid increase.

Above Izãna, all the model simulations underestimate the stratospheric N_2O columns with respect to the FTIR observations, with the largest difference reaching 14% for MERRA2. Concerning ACE-FTS, the bias with FTIR measurements is around 8%, which is qualitatively consistent with the results of Strong et al. (2008), even though they used v2.2 of ACE-FTS. However, García et al. (2021) showed good agreement above Izãnafor tropospheric N_2O abundances and total N_2O columns obtained from independent measurements. The difference between the stratospheric N_2O columns measured by FTIR and ACE-FTS could be explained by the poor coverage of ACE-FTS over the tropical and subtropical regions. Since the ACE-FTS measurements represent a latitude band, the observed N_2O results biased towards the values measured at higher latitudes, where more occultations are available (Kolonjari et al., 2018). Since the N_2O abundances decrease poleward (Jin et al., 2009), this could explain the low bias in the stratospheric N_2O columns measured by ACE-FTS compared to those obtained from FTIR.

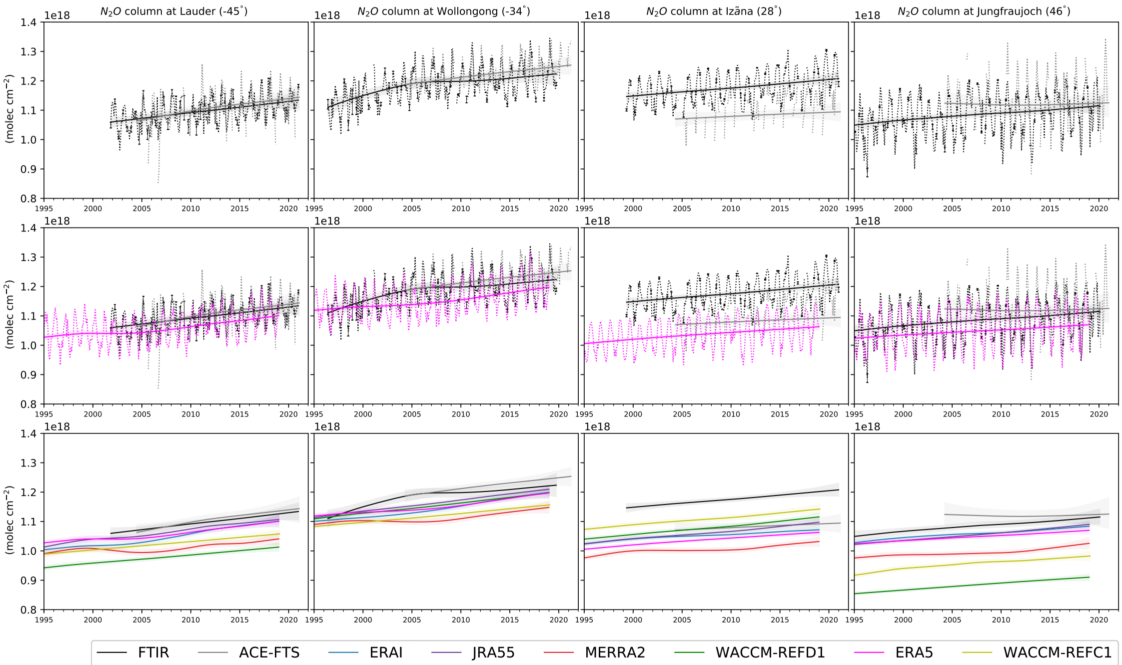

Figure 1. Time-series of N_2O stratospheric columns (12-40 km) from observations and models at four stations. Continuous lines show the linear fit obtained by the DLM regression, dashed lines depict the N_2O column data. The color code is shown in the legend. First row: DLM fits and data for FTIR and ACE-FTS measurements. Second row: DLM fits and data for FTIR and ACE-FTS measurements and the BASCOE simulation driven by ERA5. Third row: DLM fits for all the datasets considered. The model and satellite data are interpolated to the longitude and latitude of the station, and vertically regridded to match the retrieval layering schemes. After the regridding, the data were smoothed using the FTIR averaging kernels. The colored shadings represent the uncertainties from the 2.5 and 97.5 percentiles of the distributions from the DLM.

Above Jungfraujoch, there is the largest spread in the linear fits of the stratospheric N_2O columns, with differences reaching around 25% between ACE-FTS and WACCM-REFD1. Prignon et al. (2019) compared lower stratospheric columns of chlorodifluoromethane (HCFC-22) between an earlier WACCM version and FTIR measurements, and showed that WACCM consistently underestimates the HCFC-22 columns compared to the FTIR measurements. Since both N_2O and HCFC-22 (which has an atmospheric lifetime of 12 years, Prignon et al., 2019) are produced at the surface and transported into the stratosphere, this underestimation in WACCM could indicate a shortcoming in simulating the accumulation of long-lived tracers in the stratosphere above Northern mid-latitudes. Indeed, Angelbratt et al. (2011) already highlighted that the stratospheric transport has a large impact on the N_2O columns above Jungfraujoch compared to stations at higher latitudes. Regarding the observational datasets, there is a considerable disagreement between the FTIR instrument and ACE-FTS before 2012, showing increasing and decreasing N_2O columns, respectively. This is in contrast with the remarkably good agreement in the SH between the two datasets. This difference between the stratospheric N_2O columns in ACE-FTS and FTIR measurements will be further addressed in Sect. 4.

In the Tropics and above the lower stratospheric mid-latitudes, the N_2O mixing ratio is inversely proportional to the mean AoA (Galytska et al., 2019). The N_2O stratospheric columns at mid-latitudes considered here are highly sensitive to the N_2O abundances in the lower stratosphere, hence the inverse relationship also holds for the stratospheric N_2O columns above the mid-latitudes. Thus, the lower N_2O stratospheric columns in MERRA2 compared to the other datasets across the stations are consistent with the older mean AoA throughout the stratosphere found using MERRA2 by Chabrillat et al. (2018). The N_2O distribution in the stratosphere is opposite also to the total inorganic fluorine F_y. N_2O is emitted in the troposphere while F_y is produced in the stratosphere, and the transport due to the BDC tends to remove N_2O and increase F_y in the stratospheric mid-latitudes. In the light of this relationship between N_2O and F_y, the underestimated N_2O columns above Lauder and Jungfraujoch in MERRA2 are consistent with larger F_y stratospheric columns in MERRA2 compared to the other reanalyses above those stations (Prignon et al., 2021).

Figure 2 shows distributions of the trend of the stratospheric N_2O columns obtained from the respective linear fits over the common period 2005-2018. The N_2O trends at the surface have already been validated for a number of FTIR stations (including Lauder, Wollongong and Izãna) against observations from flask samples, showing an excellent agreement (Zhou et al., 2019).

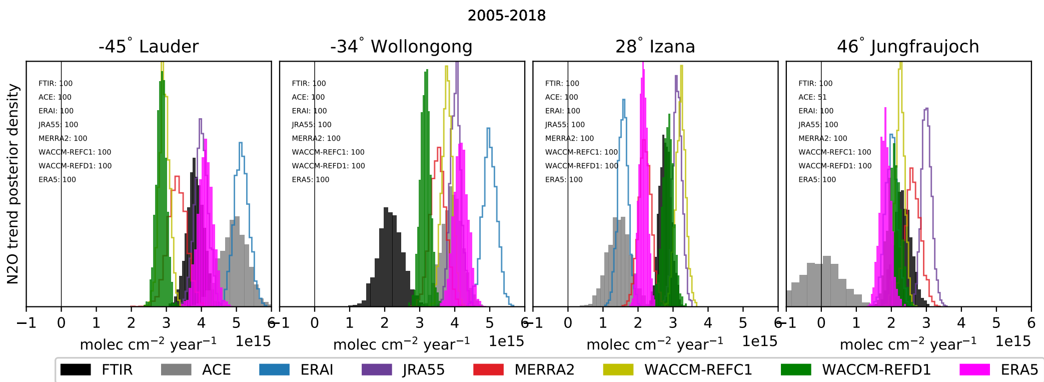

Figure 2. Posterior probability of positive changes of the DLM linear trend of the stratospheric N_2O columns (12-40 km) for the four FTIR stations (2005-2018). The color code is shown in the legend.

Above Lauder, the N_2O trends obtained with ERA5 are in good agreement with the FTIR measurements, but are underestimated in WACCM-REFD1 (around 25%) with no particular improvement with respect to WACCM-REFC1. At Wollongong, the N_2O trend obtained with the FTIR measurements is the smallest because the N_2O increase above that station is smoother compared to the other datasets. Interestingly, the N_2O trend simulated by WACCM-REFD1 is the closest to the trend obtained from the FTIR observations, while the trend obtained with ERA5 is almost twice as large. Above Izãna, WACCM-REFD1 agrees remarkably well with the FTIR (difference around 3%), while the trend from ERA5 lies between the trends measured from FTIR and ACE-FTS, with around 20% difference compared to FTIR. Above Jungfraujoch, the trend in the N_2O columns from WACCM-REFD1 agrees with the trend from the FTIR station within 10% difference and is similar to what is obtained with ERA5. The decreasing N_2O stratospheric column in ACE-FTS before 2012 results in a near-zero trend, which is in contrast with the trends obtained by the other datasets, which approximately range from 2 to 3×10^{15} molec cm^{-2} year $^{-1}$.

Considering decadal changes, the observations and the ERA5 simulation show larger trends of the stratospheric N_2O columns in the SH than in the NH, especially at mid-latitudes (respectively Lauder and Jungfraujoch). WACCM-REFD1 also shows this hemispheric difference at mid-latitudes, which is a clear improvement with respect to WACCM-REFC1. Those asymmetries are consistent with the results of Strahan et al. (2020), who found significantly negative AoA trends in the SH compared to the NH using HCl and HNO_3 measured at several ground-based FTIR stations. In addition, the hemispheric differences of the N_2O trends are also consistent with the results of Prignon et al. (2021), who found larger and more significant Fy trends above Jungfraujoch than above Lauder.

We conclude the section by providing a short description of the limits of using stratospheric columns of N_2O from FTIR measurements. As mentioned earlier, the stratospheric N_2O columns between 12 and 40 km are primarily influenced by the steady increase in the lowermost stratosphere. The DOFS of the FTIR instrument at Jungfraujoch for the stratosphere (12-40 km) is close to 1.1. Thus, the measurements cannot resolve more than one partial column between 12 and 40 km, which can hinder the detection of N_2O trends in the middle and upper stratosphere (i.e., above 30 km) because of the influence of the increase in the lowermost stratosphere. Indeed, it was shown that stratospheric N_2O trends over the last decades, obtained both from satellite measurements and model simulations, do not consist of just a global increase, but largely depend on latitude and height (e.g., Froidevaux et al., 2019). Therefore, we will consider latitudinal- and vertical-dependent trends of N_2O mixing ratios in the following section.

4 Global N_2O Linear Trends

Figure 3 shows latitude-vertical cross sections of the linear trends of the N_2O mixing ratios for the various datasets, over the 2005-2018 period. In order to perform a fair comparison, the model datasets are sampled in space and time as ACE-FTS before the computation of the trends. We use the ACE-FTS measurements as a reference, because they encompass this relatively long period with global coverage and good stability (P. Bernath et al., 2020, 2021).

In the upper stratosphere above 10 hPa, the N_2O trends from ACE-FTS are positive, with larger trends in the NH that are found significant at lower levels than in the SH. The ERAI-driven simulation qualitatively reproduces these patterns in the upper stratosphere, while the other model datasets differ from ACE-FTS, especially ERA5. A common feature among all datasets is an increase in N_2O above the Equator in the upper stratosphere, around 5 hPa. At those altitudes of the tropical pipe, the upward trans-

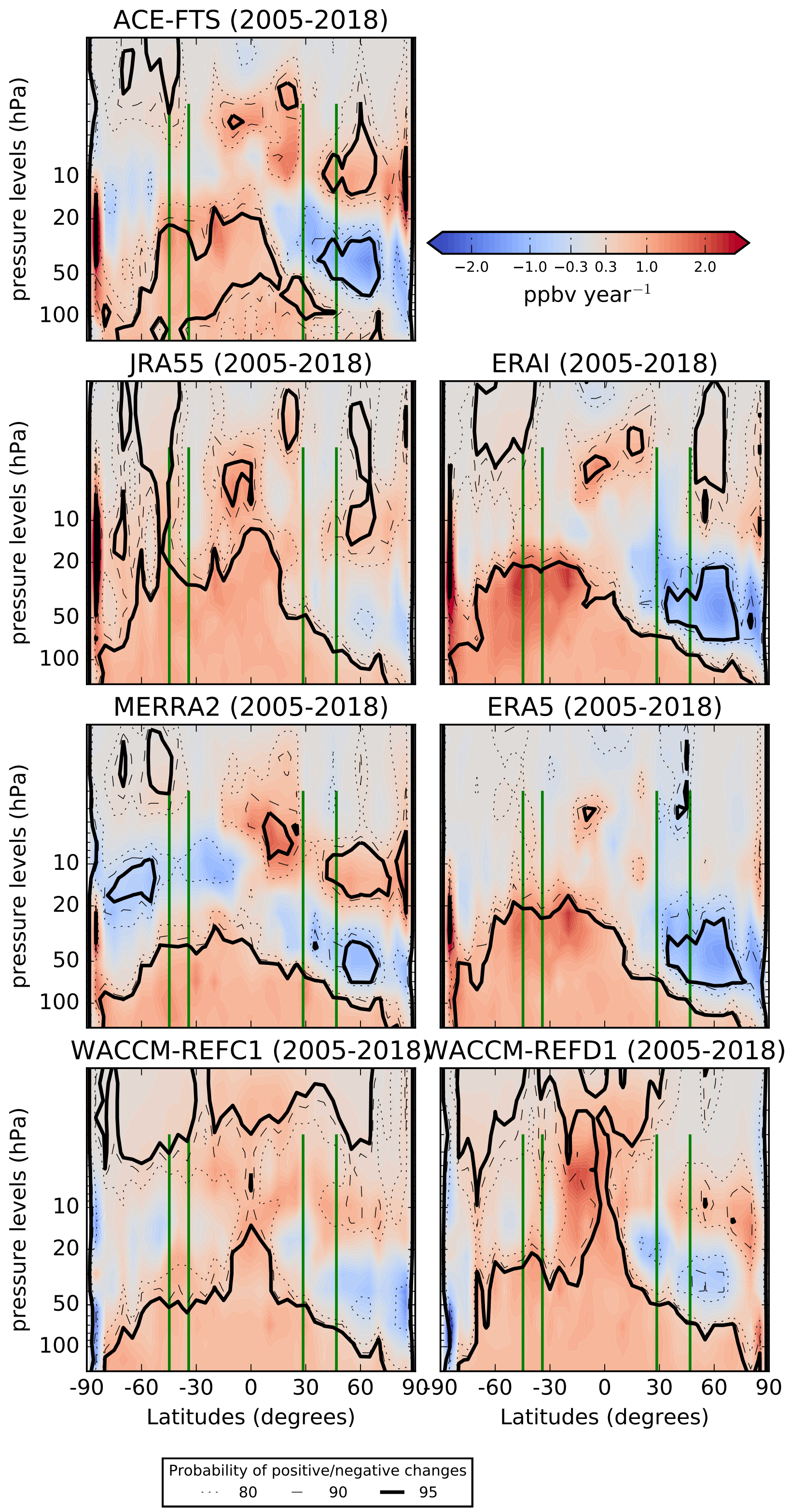

Figure 3. Latitude-pressure cross-sections of N_2O linear trends (pptv year^{-1}) obtained from the DLM (2005-2018). The N_2O simulated by the model is interpolated to the location and timing of the observations, see text for details. The dotted, dashed and continue lines represent the probability at 80, 90 and 95% of positive/negative N_2O changes respectively. The green vertical lines identify the position of the FTIR stations together with their vertical coverage.

port of N_2O by the mean advection reaches its maximum (see M2020). In the mid-lower stratosphere below 20 hPa, ACE-FTS shows a clear hemispherical asymmetry (meridional dipole) in the N_2O trends, with significantly negative values in the NH and significantly positive in the SH, that is generally reproduced by the models with ERAI and ERA5 delivering trends that are most similar to those derived from ACE-FTS.

Prignon et al. (2021) used the same simulations as the present study to investigate global stratospheric trends of total inorganic fluorine Fy. The dipoles obtained here in the N_2O trends from ACE-FTS and the ECMWF reanalyses are consistent with the opposite trends of Fy for almost the same period (Prignon et al., 2021). Above the location of Jungfraujoch (the most northern vertical green line), the negative N_2O trend detected by ACE-FTS in the mid-lower stratosphere is responsible for the disagreement with the FTIR observations discussed in the previous section, as the layer of the stratospheric N_2O column encompasses regions of both positive (lowermost and upper stratosphere) and negative (mid-lower stratosphere) N_2O trends. In the lowermost stratosphere (pressure larger than 100 hPa), all models and ACE-FTS show positive N_2O trends, resulting from the constant increase in the troposphere. However, the N_2O increase in the equatorial lowermost stratosphere is not significant in ACE-FTS, contrary to the model simulations.

Figure 4 shows the N_2O trends as in Fig. 3, but in the model space, i.e., the sampling from the observations is not applied. A comparison between each model simulation in the observation and model space (respectively Fig. 3 and Fig. 4) reveals large differences in the N_2O decadal trends. Generally, the sampling of the ACE-FTS observations enhances the trends simulated by the models, both in the negative and positive directions. For the ERA5 simulation, the significantly negative trend in the NH observational space becomes insignificant in model space. In addition, one notes immediately that the N_2O trends in the WACCM simulations change sign, with negative trends in the NH in the observational space becoming weakly positive in model space. However, this difference is not significant because neither of the trends above that region is statistically significant at 95%.

For satellite measurements, the impact of the sampling in the detection of trends in long-lived species (including N_2O) has been evaluated in Millán et al. (2016). They concluded that large errors may arise in the detected trends for coarse and non-uniform sampling obtained with occultation instruments (such as ACE-FTS), and that long time scales are required for a robust trend detection from these datasets. Such errors propagate to the models when they are sampled in space and time as the observations. In particular, within the DLM, the non-uniform time sampling considerably increases the standard deviation of the error in the time series, which is zero for regular time sampling. This difference plays a role when deriving trends over these relatively short (decadal) time scales. For example, the non-uniform ACE-FTS sampling applied to the ERA5 output results in negative N_2O trends that are 4 times stronger compared to the native grid above the northern mid-latitudes between 50 and 70 hPa. For WACCM, the issue of downsampling was also raised by Garcia et al. (2011) when comparing AoA trends obtained from balloon-borne observations and simulated by the model. They showed that sampling the model as the observations would deliver positive and non-significant AoA trends, similarly to the observations. We find consistent results with the WACCM simulations: sampling the WACCM output as the observations drives the N_2O trends towards the observed values. In addition, the non-significant negative N_2O trends simulated by WACCM are compatible with the non-significant positive AoA trends found by Garcia et al. (2011) when downsampling WACCM at the AoA observations. Hence, the ACE-FTS sampling exaggerates the simulated N_2O trends in the stratosphere.

In order to understand the actual trends and compare them with other modeling studies, we now focus on the N_2O trends obtained from the model datasets in model space (Fig. 4). We mentioned earlier that the mean AoA and the N_2O abundancies are inversely

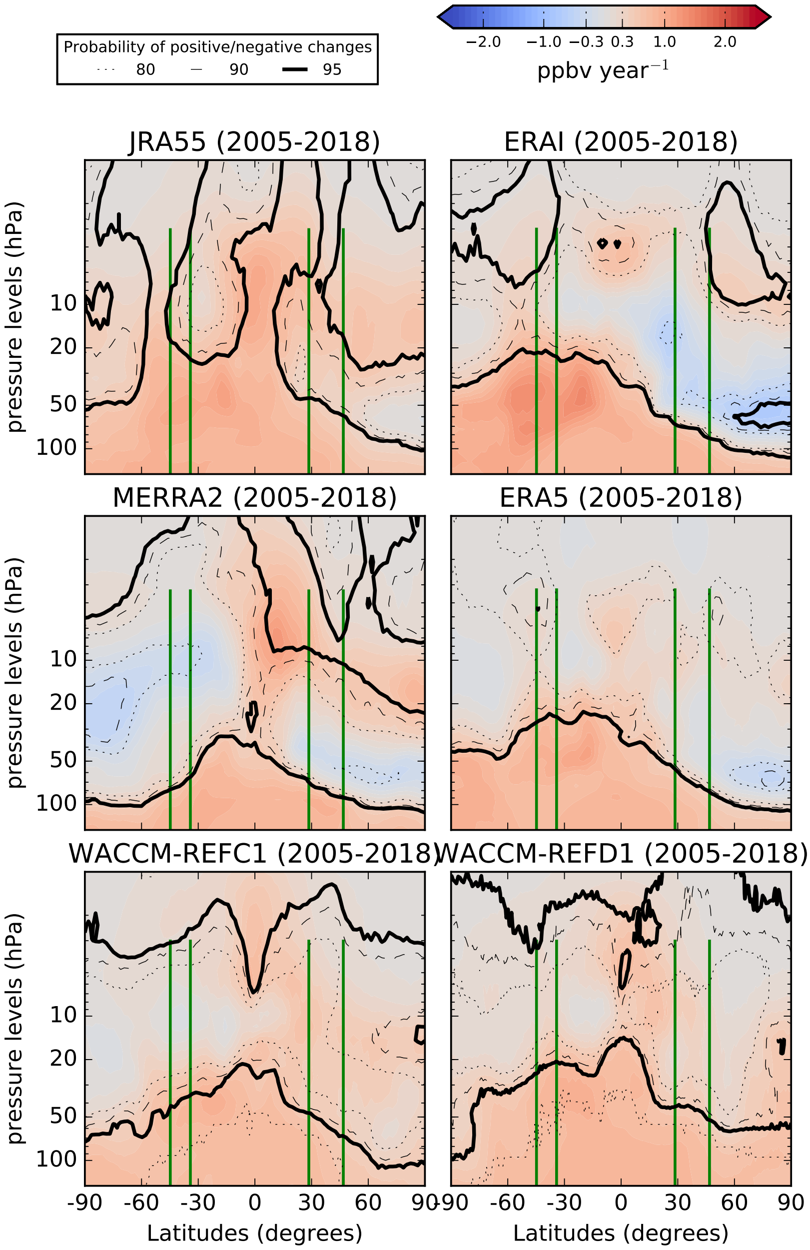

Figure 4. As in Figure 3, but in the model space.

correlated in the Tropics and above the lower stratospheric mid-latitudes. Thus, the stratospheric N_2O trends have opposite signs compared to trends of mean AoA. For ERAI, the meridional N_2O trend dipole is consistent with AoA trends derived over a shorter period with the same CTM (Chabrillat et al., 2018) and also with different CTMs (Ploeger et al., 2019; Han et al., 2019). ERAI shows positive N_2O trends in the upper stratosphere, around 5 hPa, above the Equator, which is consistent with the findings of Galytska et al. (2019) using the same reanalysis to drive a different CTM in that region, but ERA5 does not allow us to find any significant trend in the upper stratosphere. The ERA5 simulation confirms the meridional dipole in the mid-lower stratosphere of ERAI, and is consistent with recent AoA trend results over a shorter period (Ploeger et al., 2021).

Above the SH mid-latitudes in the mid-lower stratosphere, the N_2O trends obtained with MERRA2 are biased low compared to the other models, and do not replicate the hemispheric asymmetry that is visible in the ECMWF reanalyses. Wargan et al. (2018) have shown that the tropopause height has changed in MERRA2 in the past decades, with a decrease in the extratropics and an increase above the Tropics. The pattern of the N_2O trends in MERRA2 is qualitatively consistent with the changing tropopause height: a rise of the tropopause would lead to positive N_2O trends, while a sinking tropopause to negative N_2O trends. In addition, the N_2O trends with MERRA2 do not match the AoA trends obtained with the same CTM (Chabrillat et al., 2018), at least in the regions where the inverse relationship between N_2O and AoA holds (Galytska et al., 2019). Ploeger et al. (2019) found that AoA trends in the stratosphere for MERRA2 are opposite with their diabatic transport model than with our kinematic transport model. The large differences between JRA55 and MERRA2 and the ECMWF reanalyses highlight the fact that decadal changes in the stratospheric transport are not as robustly detected in JRA55 and MERRA2 as in the ERAI and ERA5. The WACCM simulations do not simulate the vertical and meridional gradients of the N_2O trends, especially compared to the CTM experiments driven by MERRA2 above the southern polar latitudes and by the ECMWF reanalyses above the northern polar latitudes, but rather a global N_2O increase that is largest in the lower stratosphere. This N_2O increase in the tropical lower stratosphere can be related to the AoA decrease due to the projected BDC acceleration in response to global warming (e.g., Butchart, 2014). However, WACCM-REFD1 improved the representation of the N_2O trends with respect to WACCM-REFC1 in the SH mid-latitudes. The newer WACCM version simulates significant N_2O increase up to 20 hPa, which makes the N_2O trends in the mid-lower stratosphere slightly more similar to the meridional dipole seen in ERAI and ERA5, even though the decreasing N_2O trends in the NH are not reproduced.

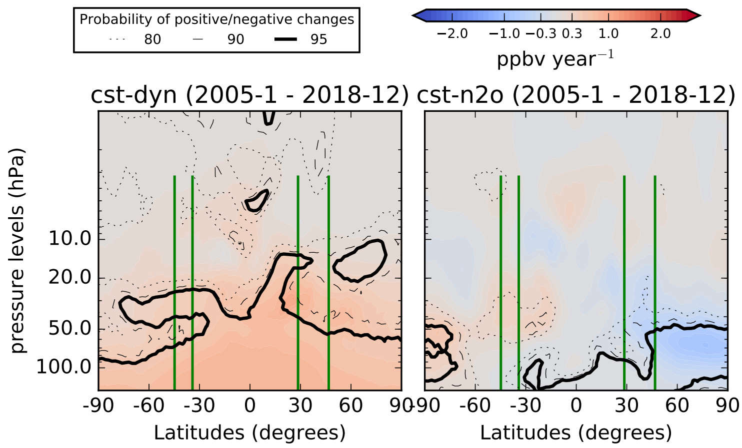

Figure 5. Latitude-pressure cross sections of N_2O linear trends (pptv year^{-1}) obtained from the DLM from a BASCOE run driven by ERA5 with fixed dynamics and increasing N_2O (left panel), and from the same model setup but with N_2O kept constant at the surface and time-varying dynamics (right panel).

The two sensitivity tests done with ERA5 (cst-dyn and cst-N_2O) are shown in Fig. 5. As expected, the cst-dyn experiment does not simulate any N_2O decrease in the stratosphere, showing only a steady N_2O increase as a consequence of the constant buildup at the surface. Between 30 and 50 hPa, the N_2O increase in the SH is significant with 95% probability, while this is not the case over the NH. This difference can be attributed to the larger variability of the NH over one QBO cycle compared to the SH due to its larger wave activity (Scaife & James, 2000), and was already shown for the significance of ozone trends (Shepherd, 2008). This highlights the importance of considering a sufficiently long period for the trend detection in the stratosphere (Garcia et al., 2011; Hardiman et al., 2017). In particular, the 14 years considered here are sufficient to propagate the N_2O increase to the mid-stratospheric mid-latitudes in the SH but not in the NH. The cst-N_2O sensitivity test confirms that the extratropical N_2O trends in the mid-lower stratosphere are due to the impact of changes in the stratospheric transport. Contrarily to the cst-dyn experiment, a changing dynamics impacts the sign of the obtained trends, with an N_2O decrease above the NH and increase in the SH. The mean stratospheric transport contributes to the hemispheric asymmetry through differences in the significance of the trends between the hemispheres, and the decadal changes in the transport contribute to the recovered trends through changes in their signs.

5 N_2O TEM Budget

This section further investigates the N_2O trends from the model simulations using the TEM budget. Equation 2 allows separating the contributions of the residual advection and mixing terms (respectively ADV and MIX) to the N_2O rate of change. In particular, we aim to identify the contributions from changes in the ADV and MIX terms to the N_2O trends shown in the previous section. To that end, we compute the changes of the ADV and MIX terms as the differences between their linear fits (i.e., the μ_t term of Eq. 3) at the end and the beginning of the considered period. A similar analysis was also done by the recent study of Abalos et al. (2020), who used the outputs of several CCMs to compute changes of the TEM budget terms of synthetic tracers. For a detailed description of the climatologies of the ADV and MIX terms, we refer to M2020.

We highlight that we do not aim to provide a quantitative analysis of the contributions of the changes of each transport term to the N_2O trends. The complete TEM budget also includes the chemistry term $\overline{S}$ (i.e., loss due to photolysis, Tian et al., 2020), which is large in the tropical mid-high stratosphere, and the residual term $\overline{\epsilon}$, which accounts for all the processes not resolved by the TEM analysis (Eq. 2). Here, we provide a qualitative estimate of the contributions from changes in the advection and mixing to the N_2O trends, by comparing the signs of the changes of ADV and MIX with those of the N_2O trends discussed in the previous section. Figure 6 shows the latitude-vertical cross sections of those changes in the ADV and MIX terms over the 2005-2018 period. We limit the analysis to the simulations by ERA5, WACCM-REFD1 and MERRA2 in order to investigate further the differences in their N_2O trends discussed in the previous section. In the following, we refer to N_2O trends discussed in the previous section as "direct" N_2O trends, in order to distinguish them from the N_2O changes derived from changes in the ADV and MIX contributions.

Looking at the changes in the ADV term in ERA5, the N_2O abundances increase in the tropical high stratosphere (between 4 and 10 hPa) because of the impact of advection, similarly to the weak positive direct N_2O trends above the same region. These changes are mainly due to an enhanced tropical upwelling over that region (not shown), and agree with a recent study showing a strengthening of the advective part of the BDC obtained from ERA5 over a longer period (Diallo et al., 2021). Above the lower stratospheric subtropics, the positive N_2O changes due to an enhanced ADV contribution are small but significant and can contribute to the positive direct N_2O trend above the SH. Such increased contribution from ADV above the lower stratospheric subtropics can be associated with the strengthening of the shallow branch of the BDC (P. Lin & Fu, 2013), which was recently detected in ERA5 using the AoA diagnostic (Ploeger et al., 2021).

Above the extratropical latitudes, the changes of the ADV term differ between the two hemispheres. Above the northern polar latitudes below 50 hPa, the negative changes of the ADV term can explain the negative direct N_2O trend and are consistent with the enhanced advection term over the tropical region. Above the southern mid-latitudes, the ADV term shows positive changes between 30 and 70 hPa. Over that region, N_2O-rich air is advected upward and southward from the lower tropical region (M2020 and their Supplement). Therefore, the positive ADV changes can indicate a strengthening of the residual advection over that region and can contribute to the positive direct N_2O trend, which is part of the hemispheric asymmetry described in the previous section.

Concerning the MIX term in ERA5, its changes are more irregular compared to those of the ADV term, and do not correspond to the direct N_2O trends over the NH. Above the SH between 10 and 30 hPa, there is enhanced poleward N_2O mixing from the subtropics (where MIX changes are negative), and increased N_2O abundances over the mid-latitudes (positive MIX changes). Such positive N_2O changes above the southern mid-latitudes can be associated with the positive but not significant direct N_2O trends over the same region. The role of mixing in the decadal BDC trends has been studied in ECMWF reanalyses, especially using AoA (e.g., Ploeger et al., 2015; Dietmüller et al., 2017). Recent studies have associated the N_2O trend dipole discussed in the previous section with a southward shift of the circulation pattern, which in turn is related to the impact of mixing on the BDC changes (Stiller et al., 2017; Ploeger et al., 2019). Our results with N_2O from ERA5 confirm the role of mixing processes above the southern mid-latitudes in determining changes in the N_2O abundances, and indirectly support the hypothesis of the southward shift of the circulation as the reason for the dipole structure. Considering AoA results, Ploeger et al. (2015) showed that mixing plays a major role in the SH in determining the negative AoA trend over the 2002-2012 period for ERAI, which is consistent with the impact of mixing on the positive N_2O changes in ERA5 outlined here.

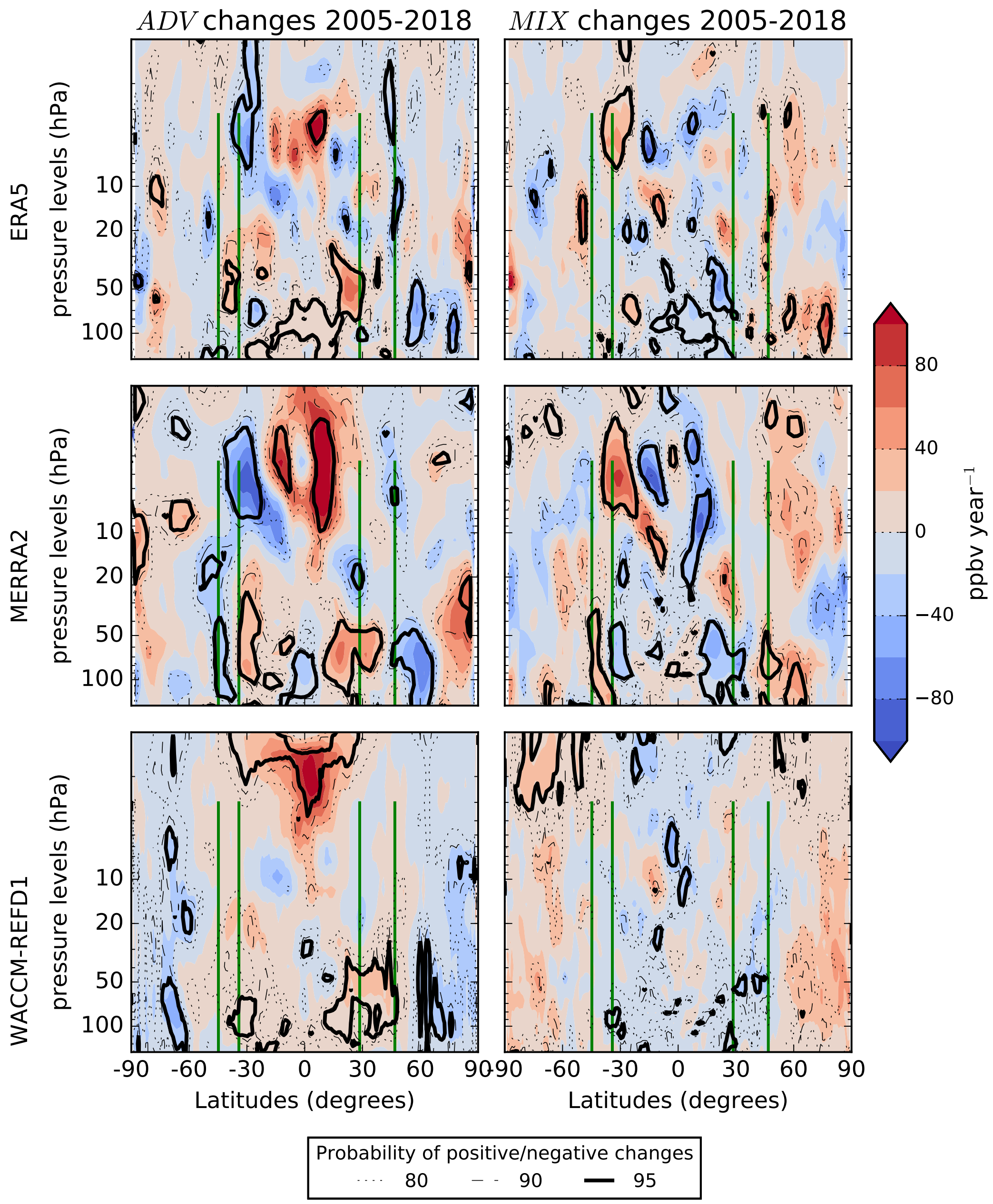

Figure 6. Latitude-pressure cross sections of the changes of the advection term (A_z+A_y, central panel, ppbv year^{-1}) and mixing term (M_z+M_y, left panel, ppbv year^{-1}) of the TEM N_2O budget for ERA5, WACCM-REFD1 and MERRA2 (2005-2018). The dotted, dashed and continue lines represent the probability at 80, 90 and 95% of positive/negative N_2O changes respectively. The green vertical lines identify the position of the FTIR stations together with their vertical coverage.

We now consider the MERRA2 simulation, starting with the changes in the *ADV* term. Similar to the ERA5 simulation, the MERRA2 experiment shows positive *ADV* changes over the tropical region above 10 hPa, which correspond to positive direct N_2O trends over the same region. These changes are due to an enhanced tropical upwelling at those levels (not shown), and qualitatively agree with the negative trends of mean AoA simulated by MERRA2 over a similar period (Ploeger et al., 2019). Above the subtropics in the lower stratosphere, the changes of the *ADV* term are positive and stronger than those obtained from the ERA5 simulation, and can be associated with the strengthening of the shallow branch of the BDC in MERRA2, as was already argued by Wargan et al. (2018). Above the southern mid-latitudes between 10 and 30 hPa, the decreasing *ADV* term leads to negative N_2O changes, indicating an enhanced downwelling over that region. Those negative *ADV* changes, possibly combined with larger chemical losses, correspond to the negative but not significant direct N_2O trends over the same region.

Regarding the *MIX* term in the MERRA2 simulation, there are no significant changes that correspond to direct N_2O trends. An intercomparison of AoA trends among reanalyses showed that significant differences in mixing exist between MERRA2 and ERAI that contribute to the mean AoA, as well as differences in the trends of the AoA spectrum in the lower and middle stratosphere (Ploeger et al., 2019). Indeed, we find large differences in the mixing contribution to the N_2O trends between MERRA2 and ERA5 (which is very similar to ERAI, not shown).

After discussing the TEM terms in the BASCOE simulations driven by ERA5 and MERRA2, we now investigate those simulated by WACCM-REFD1, starting with the *ADV* contribution. Similar to the BASCOE experiments, the positive changes in the *ADV* term simulated by WACCM-REFD1 consistently result in an N_2O increase in the Tropics above 5 hPa, which contributes to the positive direct N_2O trend over the same region. In addition, the *ADV* term is also enhanced above the subtropical lower stratosphere, possibly as a consequence of the strengthening of the shallow branch of the BDC that was robustly detected in CCMs (Butchart, 2014). Above the polar latitudes of both hemispheres, the *ADV* term decreases, resulting in negative N_2O changes, which are not visible in the direct N_2O trends because masked by the constant N_2O increase in the lowermost stratosphere. These patterns of positive and negative N_2O changes due to changes in the *ADV* term across the whole stratosphere are driven by a strengthening of the upwelling in the Tropics and downwelling in the extratropics (not shown), and can be associated with the acceleration of the BDC, which was robustly detected in several CCMs studies over longer periods (e.g., Abalos et al., 2021).

The changes in the *MIX* term in WACCM-REFD1 have a small impact on the N_2O trends compared to those of the *ADV* term. Large differences between WACCM and reanalyses were shown already by M2020 for WACCM-REFC1 for the climatologies of the mixing terms of the TEM budget. Furthermore, the weaker effect of mixing in WACCM-REFD1 compared to ERA5 is consistent with AoA studies that found weaker trends in aging by mixing in a free-running CCM compared to its specified-dynamics version and a reanalysis (Dietmüller et al., 2017).

From this section, we highlight that, within the TEM framework, changes in the residual advection have a stronger impact on the direct N_2O trends compared to those in mixing, for all datasets. However, the ERA5 simulation also delivers significant N_2O changes due to mixing that are consistent with previous studies using ECMWF reanalysis. We also notice that the hemispheric asymmetry in the direct N_2O trends simulated by ERA5 can be attributed to changes in both advection and mixing.

6 Summary and Conclusions

We have investigated the N_2O stratospheric columns (12-40 km) and their decadal (2005-2018) rates of change at four ground-based FTIR stations: Lauder (45°S), Wollongong (34°S), Izãna (28°N) and Jungfraujoch (46°N). We compared those ground-based observations with space-borne measurements from ACE-FTS, with the output of the BASCOE CTM driven by four modern reanalyses: ERAI, ERA5, JRA55 and MERRA2, and with two versions of WACCM: WACCM-REFC1 (version 4) and WACCM-REFD1 (version 6). We also studied the latitudinal and vertical distributions of these trends of the N_2O mixing ratios from model output and satellite measurements, both in the observation and model space, and used the Transformed Eulerian Mean (TEM) budget to investigate further the trends above the SH mid-latitudes in the BASCOE CTM driven by ERA5 and MERRA2 and in WACCM-REFD1.

The comparison of the stratospheric N_2O columns reveals a good agreement above Wollongong, and Lauder to a lesser extent, and larger differences above Jungfraujoch and Izãna. The trends in the N_2O stratospheric columns are larger in the SH compared to the NH, which is consistent with hemispherical differences in trends of stratospheric tracers measured at FTIR stations over the past decade (Strahan et al., 2020; Prignon et al., 2021). We find that the decadal trends in the N_2O columns are consistently positive in all cases except for ACE-FTS observations above Jungfraujoch. However, the vertical resolution of the FTIR retrievals above the Northern Hemisphere for N_2O limits our analysis to one stratospheric column, hence (in this analysis) the detection of potentially negative N_2O trends in the mid-stratosphere is hindered by the large N_2O increase in the lowermost stratosphere which arises from its continuous increase at the surface.

Global and vertically resolved trends of N_2O volume mixing ratios provide a more detailed picture compared to N_2O profiles obtained from FTIR measurements. The ACE-FTS measurements show a meridional dipole in the N_2O trends in the mid-lower stratosphere, with negative values in the NH mid-latitudes and positive values in the SH. When applying the temporal and spatial sampling of ACE-FTS on model datasets, ERAI and ERA5 compare best with the satellite measurements while the other reanalyses and the CCMs do not reproduce the meridional dipole in the mid-lower stratosphere as clearly as the ECMWF reanalyses. However, this application of the irregular sampling of ACE-FTS to the model output consistently enhances the N_2O trends, both positive and negative. Using continuous time sampling on native model grids, ERAI, and ERA5 to a lesser extent, still simulate the meridional dipole in the N_2O trends, consistently with a large number of modeling studies using both idealized and real tracers (e.g., Chabrillat et al., 2018; Ploeger et al., 2021; Prignon et al., 2021), but MERRA2, JRA55 and WACCM fail to reproduce the meridional dipole. WACCM-REFD1 is still an improvement compared to WACCM-REFC1, because it simulates the positive trend above the SH mid-latitudes also in the mid-lower stratosphere. The inherently limited spatial and temporal sampling of ACE-FTS, and its effect on N_2O trends, highlight how a regular coverage in the measurements, as in MLS, is essential to deliver reliable trends of long-lived tracers in the stratosphere. Because of this, the N_2O trends discussed here should be revisited using a newer version of MLS, once its drift in the N_2O retrievals will have been corrected.

We carried out two sensitivity tests using the BASCOE CTM driven by ERA5: one keeping N_2O constant at the surface with time-dependent dynamics (cst-N_2O), and the other using fixed dynamics with increasing N_2O at the surface (cst-dyn). The cst-N_2O experiment confirms that the extratropical N_2O trends in the mid-lower stratosphere are due to the impact of changes in the stratospheric transport. As expected, the cst-dyn simulation shows that N_2O increases everywhere, but the trend over 2005-2018 is not significantly positive in the NH mid-stratosphere. From these sensitivity tests with ERA5, we confirm that the hemispheric asymmetry of the decadal N_2O trends arises from decadal changes in transport. For the 2005-2018 period and in the 20-50 hPa layer, the hemispheric asymmetry in the significance of these trends arises from the larger dynamical variability which is found in the northern extratropics on shorter timescales, i.e. with one single QBO cycle repeating indefinitely.

We found a strong impact of transport on the stratospheric trends of N_2O volume mixing ratios for the ERA5 simulations and large differences between ERA5, MERRA2 and WACCM-REFD1. This prompted us to study the TEM budget of N_2O in these datasets, in order to separate the possible impacts of the residual advection and mixing. For all datasets, the analysis of the TEM budget reveals positive N_2O changes in the tropical mid-high stratosphere and negative changes in the northern extratropical lower stratosphere, as a result of enhanced tropical upwelling and extratropical downwelling, respectively. This is in agreement with the acceleration of the advective part of the BDC over this relatively short period both in models (Butchart, 2014) and reanalyses (Ploeger et al., 2019). For the ERA5 simulation, the positive N_2O trend above the southern midlatitudes (part of the meridional dipole) can be due to the impact of changes in both advection and mixing, the latter is consistent with previous studies, both using Age of Air (AoA, Ploeger et al., 2015) and N_2O (Stiller et al., 2017). The TEM budget obtained with MERRA2 delivers different results, with a larger impact of the residual advection in forcing the N_2O trends. This discrepancy is consistent with the large differences between MERRA2 and other reanalyses when considering stratospheric mixing on decadal time scales (e.g., Ploeger et al., 2019).

Using a measurable tracer for stratospheric transport studies allows direct comparisons with observations. The rate of change of N_2O at the surface is well-known and approximately linear and the chemical losses are limited to the higher stratosphere. In theory, this relatively simple chemistry, combined with its long life, makes N_2O a very good tracer for stratospheric transport studies. Unfortunately, no ideal observational dataset currently exists for N_2O-based investigations such as the present study: FTIR observations generally lack adequate vertical resolution, the N_2O product from the latest MLS version suffers from an unrealistic drift, and ACE-FTS has poor spatial and temporal sampling. Here, we showed how model studies of N_2O trends still provide new insights about the BDC and its changes thanks to properly taking into account the ACE-FTS sampling, complementary sensitivity tests, and the TEM analysis. Despite the shortcomings of the TEM approach, i.e., the difficulty of closing its budget, its combination with sensitivity tests provides new insights on transport changes and their impacts on the composition of the stratosphere. This approach could be extended to other tracers that are both measured and modeled - e.g., carbon monoxide, methane, and inorganic fluorine.

Acknowledgments

We thank P. Bernath for his leadership of the ACE mission, which is supported by the Canadian Space Agency. Measurements at Lauder are core-funded by the National Institute of Water and Atmospheric Research Ltd. (NIWA) through New Zealand's Ministry of Business, Innovation and Employment Strategic Science Investment Fund. The ULiège team is grateful to the International Foundation High Altitude Research Stations Jungfraujoch and Gornergrat (HFSJG, Bern) for supporting the facilities needed to perform the FTIR observations at Jungfraujoch. D. Minganti and M. Prignon were financially supported by the Fonds de la Recherche Scientifique (F.R.S.-FNRS, Brussels) through the ACCROSS research project (Grant no. PDR.T.0040.16). The University of Liège contribution was further supported by the GAW-CH program of MeteoSwiss and by the F.R.S.-FNRS Grant no J.0126.21. E. Mahieu is a senior research associate with the F.R.S.-FNRS. D. Kinnison was funded in part by National Aeronautics and Space Administration (NASA) grant (NNH19ZDA001N-AURAST). This research was enabled by the computational and storage resources of NCAR's Computational and Information Systems Laboratory (CISL), sponsored by the NSF. Cheyenne: HPE/SGI ICE XA System (NCAR Community Computing). Boulder, CO: National Center for Atmospheric Research. https://doi.org/10.5065/D6RX99HX. The WACCM and BASCOE CTM data used for the N_2O

trends and TEM comparisons in the study are available at the BIRA-IASB repository (`http://repository.aeronomie.be`) via https://dx.doi.org/10.18758/71021071 with CC BY license (Minganti & Errera, 2022). FTIR data at the various stations are available at `https://www-air.larc.nasa.gov/pub/NDACC/PUBLIC/stations/`. ACE-FTS data are available at `https://databace.scisat.ca/level2/ace_v4.1/display_data.php`. ERA5 data are available at `https://cds.climate.copernicus.eu/`. ERA-Interim data are available at `https://apps.ecmwf.int/datasets/`. JRA-55 data are available at `https://rda.ucar.edu/`. MERRA2 data are available at `https://disc.gsfc.nasa.gov/datasets/`. The DLM source code is available at `https://github.com/justinalsing/dlmmc`.

References

Abalos, M., Calvo, N., Benito-Barca, S., Garny, H., Hardiman, S. C., Lin, P., ... others (2021). The Brewer-Dobson circulation in CMIP6. *Atmospheric Chemistry and Physics Discussions*, 1–27.

Abalos, M., Orbe, C., Kinnison, D. E., Plummer, D., Oman, L. D., Jöckel, P., ... others (2020). Future trends in stratosphere-to-troposphere transport in CCMI models. *Atmospheric chemistry and physics*, *20*(11), 6883–6901.

Abalos, M., Randel, W., Kinnison, D., & Serrano, E. (2013). Quantifying tracer transport in the tropical lower stratosphere using WACCM. *Atmos. Chem. Phys*, *13*(10), 591–10.

Alsing, J. A. (2019). dlmmc: Dynamical linear model regression for atmospheric time-series analysis. *Journal of Open Source Software*, *4*(37), 1157.

Andrews, D. G., Holton, J. R., & Leovy, C. B. (1987). *Middle atmosphere dynamics* (No. 40). Academic press.

Angelbratt, J., Mellqvist, J., Blumenstock, T., Borsdorff, T., Brohede, S., Duchatelet, P., ... Urban, J. (2011). A new method to detect long term trends of methane (CH_4) and nitrous oxide (N_2O) total columns measured within the NDACC ground-based high resolution solar FTIR network. *Atmospheric Chemistry and Physics*, *11*(13), 6167–6183. Retrieved from `https://acp.copernicus.org/articles/11/6167/2011/` doi: 10.5194/acp-11-6167-2011

Bader, W., Bovy, B., Conway, S., Strong, K., Smale, D., Turner, A. J., ... Mahieu, E. (2017). The recent increase of atmospheric methane from 10 years of ground-based ndacc ftir observations since 2005. *Atmospheric Chemistry and Physics*, *17*(3), 2255–2277. Retrieved from `https://acp.copernicus.org/articles/17/2255/2017/` doi: 10.5194/acp-17-2255-2017

Baldwin, M., Gray, L., Dunkerton, T., Hamilton, K., Haynes, P., Randel, W., ... others (2001). The quasi-biennial oscillation. *Reviews of Geophysics*, *39*(2), 179–229.

Ball, W. T., Alsing, J., Mortlock, D. J., Rozanov, E. V., Tummon, F., & Haigh, J. D. (2017). Reconciling differences in stratospheric ozone composites. *Atmospheric Chemistry and Physics*, *17*(20), 12269–12302. Retrieved from `https://acp.copernicus.org/articles/17/12269/2017/` doi: 10.5194/acp-17-12269-2017

Ball, W. T., Alsing, J., Mortlock, D. J., Staehelin, J., Haigh, J. D., Peter, T., ... Rozanov, E. V. (2018). Evidence for a continuous decline in lower stratospheric ozone offsetting ozone layer recovery. *Atmospheric Chemistry and Physics*, *18*(2), 1379–1394. Retrieved from `https://acp.copernicus.org/articles/18/1379/2018/` doi: 10.5194/acp-18-1379-2018

Bernath, P. (2017). The atmospheric chemistry experiment (ACE). *Journal of Quantitative Spectroscopy and Radiative Transfer*, *186*, 3-16. Retrieved from `https://www.sciencedirect.com/science/article/pii/S0022407316300176` (Satellite Remote Sensing and Spectroscopy: Joint ACE-Odin Meeting, October 2015) doi: https://doi.org/10.1016/j.jqsrt.2016.04.006

Bernath, P., Crouse, J., Hughes, R., & Boone, C. (2021). The Atmospheric Chemistry Experiment Fourier transform spectrometer (ACE-FTS) version 4.1 retrievals: Trends and seasonal distributions. *Journal of Quantitative Spectroscopy and Radiative Transfer*, *259*, 107409.

Bernath, P., Steffen, J., Crouse, J., & Boone, C. (2020). Sixteen-year trends in atmospheric trace gases from orbit. *Journal of Quantitative Spectroscopy and Radiative Transfer*, *253*, 107178. Retrieved from `https://www.sciencedirect.com/science/article/pii/S0022407320302958` doi: https://doi.org/10.1016/j.jqsrt.2020.107178

Bernath, P. F., McElroy, C. T., Abrams, M. C., Boone, C. D., Butler, M., Camy-Peyret, C., ... Zou, J. (2005). Atmospheric chemistry experiment (ACE): Mission overview. *Geophysical Research Letters*, *32*(15). Retrieved from https://agupubs.onlinelibrary.wiley.com/doi/abs/10.1029/2005GL022386 doi: https://doi.org/10.1029/2005GL022386

Butchart, N. (2014). The Brewer-Dobson circulation. *Reviews of Geophysics*, *52*(2), 157-184. Retrieved from https://agupubs.onlinelibrary.wiley.com/doi/abs/10.1002/2013RG000448 doi: https://doi.org/10.1002/2013RG000448

Butchart, N., & Scaife, A. A. (2001). Removal of chlorofluorocarbons by increased mass exchange between the stratosphere and troposphere in a changing climate. *Nature*, *410*(6830), 799–802.

Chabrillat, S., Vigouroux, C., Christophe, Y., Engel, A., Errera, Q., Minganti, D., . . . Mahieu, E. (2018). Comparison of mean age of air in five reanalyses using the BASCOE transport model. *Atmospheric Chemistry and Physics*, *18*(19), 14715–14735.

Danabasoglu, G., Lamarque, J.-F., Bacmeister, J., Bailey, D., DuVivier, A., Edwards, J., . . . others (2020). The community earth system model version 2 (CESM2). *Journal of Advances in Modeling Earth Systems*, *12*(2).

Dee, D. P., Uppala, S., Simmons, A., Berrisford, P., Poli, P., Kobayashi, S., . . . others (2011). The ERA-interim reanalysis: Configuration and performance of the data assimilation system. *Quarterly Journal of the royal meteorological society*, *137*(656), 553–597.

De Mazière, M., Thompson, A. M., Kurylo, M. J., Wild, J. D., Bernhard, G., Blumenstock, T., . . . others (2018). The Network for the Detection of Atmospheric Composition Change (NDACC): history, status and perspectives. *Atmospheric Chemistry and Physics*, *18*(7), 4935–4964.

de Wit, T. D., Bruinsma, S., & Shibasaki, K. (2014). Synoptic radio observations as proxies for upper atmosphere modelling. *Journal of Space Weather and Space Climate*, *4*, A06.

Dhomse, S. S., Kinnison, D., Chipperfield, M. P., Salawitch, R. J., Cionni, I., Hegglin, M. I., . . . Zeng, G. (2018). Estimates of ozone return dates from Chemistry-Climate Model Initiative simulations. *Atmospheric Chemistry and Physics*, *18*(11), 8409–8438. Retrieved from https://acp.copernicus.org/articles/18/8409/2018/ doi: 10.5194/acp-18-8409-2018

Diallo, M., Ern, M., & Ploeger, F. (2021). The advective brewer–dobson circulation in the era5 reanalysis: climatology, variability, and trends. *Atmospheric Chemistry and Physics*, *21*(10), 7515–7544.

Dietmüller, S., Eichinger, R., Garny, H., Birner, T., Boenisch, H., Pitari, G., . . . others (2018). Quantifying the effect of mixing on the mean age of air in ccmval-2 and ccmi-1 models. *Atmospheric Chemistry and Physics*, *18*(9), 6699–6720.

Dietmüller, S., Garny, H., Plöger, F., Jöckel, P., & Cai, D. (2017). Effects of mixing on resolved and unresolved scales on stratospheric age of air. *Atmospheric chemistry and physics*, *17*(12), 7703–7719.

Durbin, J., & Koopman, S. J. (2012). *Time series analysis by state space methods.* Oxford university press.

Eichinger, R., Dietmüller, S., Garny, H., Šácha, P., Birner, T., Bönisch, H., . . . others (2019). The influence of mixing on the stratospheric age of air changes in the 21st century. *Atmospheric chemistry and physics*, *19*(2), 921–940.

Engel, A., Bönisch, H., Ullrich, M., Sitals, R., Membrive, O., Danis, F., & Crevoisier, C. (2017). Mean age of stratospheric air derived from AirCore observations. *Atmospheric Chemistry and Physics*, *17*(11), 6825–6838.

Engel, A., Möbius, T., Bönisch, H., Schmidt, U., Heinz, R., Levin, I., . . . others (2009). Age of stratospheric air unchanged within uncertainties over the past 30 years. *Nature Geoscience*, *2*(1), 28–31.

Errera, Q., Chabrillat, S., Christophe, Y., Debosscher, J., Hubert, D., Lahoz, W., . . . Walker, K. (2019). Technical note: Reanalysis of Aura MLS Chemical Observations. *Atmospheric Chemistry and Physics Discussions*, *2019*, 1–60.

Retrieved from https://www.atmos-chem-phys-discuss.net/acp-2019-530/ doi: 10.5194/acp-2019-530

Eyring, V., Bony, S., Meehl, G. A., Senior, C. A., Stevens, B., Stouffer, R. J., & Taylor, K. E. (2016). Overview of the coupled model intercomparison project phase 6 (cmip6) experimental design and organization. *Geoscientific Model Development*, *9*(5), 1937–1958.

Fritsch, F., Garny, H., Engel, A., Bönisch, H., & Eichinger, R. (2020). Sensitivity of age of air trends to the derivation method for non-linear increasing inert SF_6. *Atmospheric Chemistry and Physics*, *20*(14), 8709–8725. Retrieved from https://www.atmos-chem-phys.net/20/8709/2020/ doi: 10.5194/acp-20-8709-2020

Froidevaux, L., Kinnison, D. E., Wang, R., Anderson, J., & Fuller, R. A. (2019). Evaluation of CESM1 (WACCM) free-running and specified dynamics atmospheric composition simulations using global multispecies satellite data records. *Atmospheric Chemistry and Physics*, *19*(7), 4783–4821. Retrieved from https://acp.copernicus.org/articles/19/4783/2019/ doi: 10.5194/acp-19-4783-2019

Fu, Q., Lin, P., Solomon, S., & Hartmann, D. (2015). Observational evidence of strengthening of the Brewer–Dobson circulation since 1980. *Journal of Geophysical Research: Atmospheres*, *120*(19), 10–214.

Fu, Q., Solomon, S., Pahlavan, H. A., & Lin, P. (2019). Observed changes in Brewer–Dobson circulation for 1980–2018. *Environmental Research Letters*, *14*(11), 114026.

Fujiwara, M., Wright, J. S., Manney, G. L., Gray, L. J., Anstey, J., Birner, T., ... others (2017). Introduction to the SPARC Reanalysis Intercomparison Project (S-RIP) and overview of the reanalysis systems. *Atmospheric Chemistry and Physics*, *17*(2), 1417–1452.

Galytska, E., Rozanov, A., Chipperfield, M. P., Dhomse, Weber, M., Arosio, C., ... Burrows, J. P. (2019). Dynamically controlled ozone decline in the tropical mid-stratosphere observed by SCIAMACHY. *Atmospheric Chemistry and Physics*, *19*(2), 767–783. Retrieved from https://www.atmos-chem-phys.net/19/767/2019/ doi: 10.5194/acp-19-767-2019

García, O. E., Schneider, M., Sepúlveda, E., Hase, F., Blumenstock, T., Cuevas, E., ... López, C. (2021). Twenty years of ground-based NDACC FTIR spectrometry at Izaña Observatory – overview and long-term comparison to other techniques. *Atmospheric Chemistry and Physics*, *21*(20), 15519–15554. Retrieved from https://acp.copernicus.org/articles/21/15519/2021/ doi: 10.5194/acp-21-15519-2021

Garcia, R. R., Randel, W. J., & Kinnison, D. E. (2011). On the determination of age of air trends from atmospheric trace species. *Journal of the Atmospheric Sciences*, *68*(1), 139–154.

Garcia, R. R., Smith, A. K., Kinnison, D. E., de la Cámara, A., & Murphy, D. J. (2017). Modification of the Gravity Wave Parameterization in the Whole Atmosphere Community Climate Model: Motivation and Results. *Journal of the Atmospheric Sciences*, *74*(1), 275 - 291. Retrieved from https://journals.ametsoc.org/view/journals/atsc/74/1/jas-d-16-0104.1.xml doi: 10.1175/JAS-D-16-0104.1

Gelaro, R., McCarty, W., Suárez, M. J., Todling, R., Molod, A., Takacs, L., ... others (2017). The modern-era retrospective analysis for research and applications, version 2 (MERRA-2). *Journal of Climate*, *30*(14), 5419–5454.

Gettelman, A., Mills, M., Kinnison, D., Garcia, R., Smith, A., Marsh, D., ... others (2019). The whole atmosphere community climate model version 6 (WACCM6). *Journal of Geophysical Research: Atmospheres*, *124*(23), 12380–12403.

Griffith, D. W. T., Deutscher, N. M., Caldow, C., Kettlewell, G., Riggenbach, M.,

& Hammer, S. (2012). A Fourier transform infrared trace gas and isotope analyser for atmospheric applications. *Atmospheric Measurement Techniques*, *5*(10), 2481–2498. Retrieved from https://amt.copernicus.org/articles/5/2481/2012/ doi: 10.5194/amt-5-2481-2012

Haenel, F. J., Stiller, G. P., von Clarmann, T., Funke, B., Eckert, E., Glatthor, N., ... Reddmann, T. (2015). Reassessment of MIPAS age of air trends and variability. *Atmospheric Chemistry and Physics*, *15*(22), 13161–13176. Retrieved from https://acp.copernicus.org/articles/15/13161/2015/ doi: 10.5194/acp-15-13161-2015

Han, Y., Tian, W., Chipperfield, M. P., Zhang, J., Wang, F., Sang, W., ... Tian, H. (2019). Attribution of the Hemispheric Asymmetries in Trends of Stratospheric Trace Gases Inferred From Microwave Limb Sounder (MLS) Measurements. *Journal of Geophysical Research: Atmospheres*, *124*(12), 6283-6293. Retrieved from https://agupubs.onlinelibrary.wiley.com/doi/abs/10.1029/2018JD029723 doi: https://doi.org/10.1029/2018JD029723

Hardiman, S. C., Butchart, N., & Calvo, N. (2014). The morphology of the Brewer–Dobson circulation and its response to climate change in CMIP5 simulations. *Quarterly Journal of the Royal Meteorological Society*, *140*(683), 1958–1965.

Hardiman, S. C., Lin, P., Scaife, A. A., Dunstone, N. J., & Ren, H.-L. (2017). The influence of dynamical variability on the observed Brewer–Dobson circulation trend. *Geophysical Research Letters*, *44*(6), 2885–2892.

Hersbach, H., Bell, B., Berrisford, P., Hirahara, S., Hornyi, A., Muoz-Sabater, J., ... Thpaut, J.-N. (2020). The ERA5 global reanalysis. *Quarterly Journal of the Royal Meteorological Society*, *146*(730), 1999-2049. Retrieved from https://rmets.onlinelibrary.wiley.com/doi/abs/10.1002/qj.3803 doi: https://doi.org/10.1002/qj.3803

Hurrell, J. W., Holland, M. M., Gent, P. R., Ghan, S., Kay, J. E., Kushner, P. J., ... others (2013). The community earth system model: a framework for collaborative research. *Bulletin of the American Meteorological Society*, *94*(9), 1339–1360.

Jin, J. J., Semeniuk, K., Beagley, S. R., Fomichev, V. I., Jonsson, A. I., McConnell, J. C., ... Dupuy, E. (2009). Comparison of cmam simulations of carbon monoxide (co), nitrous oxide (n_2o), and methane (ch_4) with observations from odin/smr, ace-fts, and aura/mls. *Atmospheric Chemistry and Physics*, *9*(10), 3233–3252. Retrieved from https://acp.copernicus.org/articles/9/3233/2009/ doi: 10.5194/acp-9-3233-2009

Kobayashi, S., Ota, Y., Harada, Y., Ebita, A., Moriya, M., Onoda, H., ... others (2015). The JRA-55 reanalysis: General specifications and basic characteristics. *Journal of the Meteorological Society of Japan. Ser. II*, *93*(1), 5–48.

Kolonjari, F., Plummer, D. A., Walker, K. A., Boone, C. D., Elkins, J. W., Hegglin, M. I., ... Stiller, G. P. (2018). Assessing stratospheric transport in the cmam30 simulations using ace-fts measurements. *Atmospheric Chemistry and Physics*, *18*(9), 6801–6828. Retrieved from https://acp.copernicus.org/articles/18/6801/2018/ doi: 10.5194/acp-18-6801-2018

Kyrölä, E., Laine, M., Sofieva, V., Tamminen, J., Päivärinta, S.-M., Tukiainen, S., ... Thomason, L. (2013). Combined sage ii–gomos ozone profile data set for 1984–2011 and trend analysis of the vertical distribution of ozone. *Atmospheric Chemistry and Physics*, *13*(21), 10645–10658.

Laine, M., Latva-Pukkila, N., & Kyrölä, E. (2014). Analysing time-varying trends in stratospheric ozone time series using the state space approach. *Atmospheric Chemistry and Physics*, *14*(18), 9707–9725.

Langerock, B., De Mazière, M., Hendrick, F., Vigouroux, C., Desmet, F., Dils, B., & Niemeijer, S. (2015). Description of algorithms for co-locating and comparing gridded model data with remote-sensing observations. *Geoscientific Model Development*, *8*(3), 911–921. Retrieved from https://gmd.copernicus.org/

articles/8/911/2015/ doi: 10.5194/gmd-8-911-2015

Lin, P., & Fu, Q. (2013). Changes in various branches of the Brewer–Dobson circulation from an ensemble of chemistry climate models. *Journal of Geophysical Research: Atmospheres*, *118*(1), 73–84.

Lin, S.-J. (2004). A "vertically lagrangian" finite-volume dynamical core for global models. *Monthly Weather Review*, *132*(10), 2293–2307.

Lin, S.-J., & Rood, R. B. (1996). Multidimensional flux-form semi-lagrangian transport schemes. *Monthly Weather Review*, *124*(9), 2046–2070.

Livesey, N. J., Read, W. G., Froidevaux, L., Lambert, A., Santee, M. L., Schwartz, M. J., ... Nedoluha, G. E. (2021). Investigation and amelioration of long-term instrumental drifts in water vapor and nitrous oxide measurements from the aura microwave limb sounder (MLS) and their implications for studies of variability and trends. *Atmospheric Chemistry and Physics*, *21*(20), 15409–15430. Retrieved from https://acp.copernicus.org/articles/21/15409/2021/ doi: 10.5194/acp-21-15409-2021

Mahieu, E., Chipperfield, M., Notholt, J., Reddmann, T., Anderson, J., Bernath, P., ... others (2014). Recent northern hemisphere stratospheric HCl increase due to atmospheric circulation changes. *Nature*, *515*(7525), 104.

Marsh, D. R., Mills, M. J., Kinnison, D. E., Lamarque, J.-F., Calvo, N., & Polvani, L. M. (2013). Climate change from 1850 to 2005 simulated in cesm1(waccm). *Journal of Climate*, *26*(19), 7372 - 7391. Retrieved from https://journals.ametsoc.org/view/journals/clim/26/19/jcli-d-12-00558.1.xml doi: 10.1175/JCLI-D-12-00558.1

Matthes, K., Marsh, D. R., Garcia, R. R., Kinnison, D. E., Sassi, F., & Walters, S. (2010). Role of the qbo in modulating the influence of the 11 year solar cycle on the atmosphere using constant forcings. *Journal of Geophysical Research: Atmospheres*, *115*(D18).

Meul, S., Dameris, M., Langematz, U., Abalichin, J., Kerschbaumer, A., Kubin, A., & Oberlnder-Hayn, S. (2016). Impact of rising greenhouse gas concentrations on future tropical ozone and UV exposure. *Geophysical Research Letters*, *43*(6), 2919-2927. Retrieved from https://agupubs.onlinelibrary.wiley.com/doi/abs/10.1002/2016GL067997 doi: https://doi.org/10.1002/2016GL067997

Meul, S., Langematz, U., Kröger, P., Oberländer-Hayn, S., & Jöckel, P. (2018). Future changes in the stratosphere-to-troposphere ozone mass flux and the contribution from climate change and ozone recovery. *Atmospheric Chemistry and Physics*, *18*(10), 7721–7738. Retrieved from https://acp.copernicus.org/articles/18/7721/2018/ doi: 10.5194/acp-18-7721-2018

Millán, L. F., Livesey, N. J., Santee, M. L., Neu, J. L., Manney, G. L., & Fuller, R. A. (2016). Case studies of the impact of orbital sampling on stratospheric trend detection and derivation of tropical vertical velocities: solar occultation vs. limb emission sounding. *Atmospheric Chemistry and Physics*, *16*(18), 11521–11534. Retrieved from https://acp.copernicus.org/articles/16/11521/2016/ doi: 10.5194/acp-16-11521-2016

Minganti, D., Chabrillat, S., Christophe, Y., Errera, Q., Abalos, M., Prignon, M., ... Mahieu, E. (2020). Climatological impact of the Brewer–Dobson circulation on the N_2O budget in WACCM, a chemical reanalysis and a CTM driven by four dynamical reanalyses. *Atmospheric Chemistry and Physics*, *20*(21), 12609–12631. Retrieved from https://acp.copernicus.org/articles/20/12609/2020/ doi: 10.5194/acp-20-12609-2020

Minganti, D., & Errera, Q. (2022). *Supplement for: N_2O rate of change as a diagnostic of the brewer-dobson circulation in the stratosphere* [dataset]. Royal Belgian Institute for Space Aeronomy. Retrieved from https://repository.aeronomie.be/?doi=10.18758/71021071 doi: https://dx.doi.org/10.18758/71021071

Monge-Sanz, B. M., Chipperfield, M. P., Dee, D. P., Simmons, A. J., & Uppala, S. M. (2013). Improvements in the stratospheric transport achieved by a chemistry transport model with ECMWF (re)analyses: identifying effects and remaining challenges. *Quarterly Journal of the Royal Meteorological Society*, *139*(672), 654-673. Retrieved from `https://rmets.onlinelibrary.wiley.com/doi/abs/10.1002/qj.1996` doi: https://doi.org/10.1002/qj.1996
Morgenstern, O., Hegglin, M. I., Rozanov, E., O'Connor, F. M., Abraham, N. L., Akiyoshi, H., ... Zeng, G. (2017). Review of the global models used within phase 1 of the chemistry–climate model initiative (ccmi). *Geoscientific Model Development*, *10*(2), 639–671. Retrieved from `https://gmd.copernicus.org/articles/10/639/2017/` doi: 10.5194/gmd-10-639-2017
Neale, R. B., Richter, J., Park, S., Lauritzen, P. H., Vavrus, S. J., Rasch, P. J., & Zhang, M. (2013). The mean climate of the Community Atmosphere Model (CAM4) in forced SST and fully coupled experiments. *Journal of Climate*, *26*(14), 5150–5168.
Oberländer-Hayn, S., Gerber, E. P., Abalichin, J., Akiyoshi, H., Kerschbaumer, A., Kubin, A., ... Oman, L. D. (2016). Is the Brewer-Dobson circulation increasing or moving upward? *Geophysical Research Letters*, *43*(4), 1772-1779. Retrieved from `https://agupubs.onlinelibrary.wiley.com/doi/abs/10.1002/2015GL067545` doi: https://doi.org/10.1002/2015GL067545
Petropavlovskikh, I., Godin-Beekmann, S., Hubert, D., Damadeo, R., Hassler, B., & Sofieva, V. (2019). SPARC/IO3C/GAW report on Long-term Ozone Trends and Uncertainties in the Stratosphere.
Ploeger, F., Abalos, M., Birner, T., Konopka, P., Legras, B., Müller, R., & Riese, M. (2015). Quantifying the effects of mixing and residual circulation on trends of stratospheric mean age of air. *Geophysical Research Letters*, *42*(6), 2047–2054.
Ploeger, F., Diallo, M., Charlesworth, E., Konopka, P., Legras, B., Laube, J. C., ... Riese, M. (2021). The stratospheric Brewer–Dobson circulation inferred from age of air in the ERA5 reanalysis. *Atmospheric Chemistry and Physics*, *21*(11), 8393–8412.
Ploeger, F., Legras, B., Charlesworth, E., Yan, X., Diallo, M., Konopka, P., ... Riese, M. (2019). How robust are stratospheric age of air trends from different reanalyses? *Atmospheric Chemistry and Physics*, *19*(9), 6085–6105.
Plumb, R. A. (2002). Stratospheric transport. *Journal of the Meteorological Society of Japan. Ser. II*, *80*(4B), 793–809.
Plummer, D., Nagashima, T., Tilmes, S., Archibald, A., Chiodo, G., Fadnavis, S., ... others (2021). Ccmi-2022: A new set of chemistry-climate model initiative (ccmi) community simulations to update the assessment of models and support upcoming ozone assessment activities. *Newsletter n 57 July 2021*, 22.
Polvani, L. M., Wang, L., Abalos, M., Butchart, N., Chipperfield, M. P., Dameris, M., ... Stone, K. A. (2019). Large Impacts, Past and Future, of Ozone-Depleting Substances on Brewer-Dobson Circulation Trends: A Multimodel Assessment. *Journal of Geophysical Research: Atmospheres*, *124*(13), 6669-6680. Retrieved from `https://agupubs.onlinelibrary.wiley.com/doi/abs/10.1029/2018JD029516` doi: https://doi.org/10.1029/2018JD029516
Prignon, M., Chabrillat, S., Friedrich, M., Smale, D., Strahan, S., Bernath, P., ... others (2021). Stratospheric fluorine as a tracer of circulation changes: comparison between infrared remote-sensing observations and simulations with five modern reanalyses. *Journal of Geophysical Research: Atmospheres*, e2021JD034995.
Prignon, M., Chabrillat, S., Minganti, D., O'Doherty, S., Servais, C., Stiller, G., ... Mahieu, E. (2019). Improved FTIR retrieval strategy for HCFC-22 ($CHClF_2$), comparisons with in situ and satellite datasets with the support of models, and determination of its long-term trend above Jungfraujoch. *Atmospheric Chemistry and Physics Discussions*.

Randel, W., & Park, M. (2019). Diagnosing observed stratospheric water vapor relationships to the cold point tropical tropopause. *Journal of Geophysical Research: Atmospheres*, *124*(13), 7018–7033.

Randel, W. J., Boville, B. A., Gille, J. C., Bailey, P. L., Massie, S. T., Kumer, J., ... Roche, A. (1994). Simulation of stratospheric N_2O in the NCAR CCM2: Comparison with CLAES data and global budget analyses. *Journal of the atmospheric sciences*, *51*(20), 2834–2845.

Rodgers, C. D. (2000). *Inverse methods for atmospheric sounding: theory and practice* (Vol. 2). World scientific.

Scaife, A., & James, I. (2000). Response of the stratosphere to interannual variability of tropospheric planetary waves. *Quarterly Journal of the Royal Meteorological Society*, *126*(562), 275–297.

Seinfeld, J. H., & Pandis, S. N. (2016). *Atmospheric chemistry and physics: from air pollution to climate change.* John Wiley & Sons.

Sheese, P. E., Walker, K. A., Boone, C. D., Bernath, P. F., Froidevaux, L., Funke, B., ... von Clarmann, T. (2017). ACE-FTS ozone, water vapour, nitrous oxide, nitric acid, and carbon monoxide profile comparisons with MIPAS and MLS. *Journal of Quantitative Spectroscopy and Radiative Transfer*, *186*, 63–80.

Shepherd, T. G. (2007). Transport in the middle atmosphere. *Journal of the Meteorological Society of Japan. Ser. II*, *85*, 165–191.

Shepherd, T. G. (2008). Dynamics, stratospheric ozone, and climate change. *Atmosphere-Ocean*, *46*(1), 117-138. Retrieved from `https://doi.org/10.3137/ao.460106` doi: 10.3137/ao.460106

Simmons, A., Soci, C., Nicolas, J., Bell, B., Berrisford, P., Dragani, R., ... others (2020). *Global stratospheric temperature bias and other stratospheric aspects of ERA5 and ERA5. 1.* European Centre for Medium Range Weather Forecasts.

Stiller, G., Clarmann, T. v., Haenel, F., Funke, B., Glatthor, N., Grabowski, U., ... others (2012). Observed temporal evolution of global mean age of stratospheric air for the 2002 to 2010 period. *Atmospheric Chemistry and Physics*, *12*(7), 3311–3331.

Stiller, G., Fierli, F., Ploeger, F., Cagnazzo, C., Funke, B., Haenel, F. J., ... Clarmann, T. v. (2017). Shift of subtropical transport barriers explains observed hemispheric asymmetry of decadal trends of age of air. *Atmospheric Chemistry and Physics*, *17*(18), 11177–11192.

Strahan, S. E., Smale, D., Douglass, A. R., Blumenstock, T., Hannigan, J. W., Hase, F., ... others (2020). Observed hemispheric asymmetry in stratospheric transport trends from 1994 to 2018. *Geophysical Research Letters*, *47*(17), e2020GL088567.

Strong, K., Wolff, M. A., Kerzenmacher, T. E., Walker, K. A., Bernath, P. F., Blumenstock, T., ... Wood, S. (2008). Validation of ACE-FTS N_2O measurements. *Atmospheric Chemistry and Physics*, *8*(16), 4759–4786. Retrieved from `https://acp.copernicus.org/articles/8/4759/2008/` doi: 10.5194/acp-8-4759-2008

Tian, H., Xu, R., Canadell, J. G., Thompson, R. L., Winiwarter, W., Suntharalingam, P., ... Yao, Y. (2020). A comprehensive quantification of global nitrous oxide sources and sinks. *Nature*, *586*(7828), 248?256. doi: 10.1038/s41586-020-2780-0

von Clarmann, T., & Grabowski, U. (2021). Direct inversion of circulation from tracer measurements–Part 2: Sensitivity studies and model recovery tests. *Atmospheric Chemistry and Physics*, *21*(4), 2509–2526.

Wargan, K., Orbe, C., Pawson, S., Ziemke, J. R., Oman, L. D., Olsen, M. A., ... Emma Knowland, K. (2018). Recent Decline in Extratropical Lower Stratospheric Ozone Attributed to Circulation Changes. *Geophysical Research Letters*, *45*(10), 5166-5176. Retrieved from `https://`

agupubs.onlinelibrary.wiley.com/doi/abs/10.1029/2018GL077406 doi: https://doi.org/10.1029/2018GL077406

Waugh, D., & Hall, T. (2002). Age of stratospheric air: Theory, observations, and models. *Reviews of Geophysics*, *40*(4), 1–1.

Wolter, K., & Timlin, M. S. (2011). El Niño/Southern Oscillation behaviour since 1871 as diagnosed in an extended multivariate ENSO index (MEI. ext). *International Journal of Climatology*, *31*(7), 1074–1087.

Zander, R., Mahieu, E., Demoulin, P., Duchatelet, P., Roland, G., Servais, C., … Rinsland, C. (2008). Our changing atmosphere: Evidence based on long-term infrared solar observations at the jungfraujoch since 1950. *Science of The Total Environment*, *391*(2), 184-195. Retrieved from https://www.sciencedirect.com/science/article/pii/S0048969707010789 (Research at Jungfraujoch - Contributions to the International conference in celebration of the 75th anniversary of the High Altitude Research Station Jungfraujoch at Interlaken, Switzerland (11-13 September, 2006)) doi: https://doi.org/10.1016/j.scitotenv.2007.10.018

Zhou, M., Langerock, B., Wells, K. C., Millet, D. B., Vigouroux, C., Sha, M. K., … De Mazière, M. (2019). An intercomparison of total column-averaged nitrous oxide between ground-based FTIR TCCON and NDACC measurements at seven sites and comparisons with the GEOS-Chem model. *Atmospheric Measurement Techniques*, *12*(2), 1393–1408. Retrieved from https://amt.copernicus.org/articles/12/1393/2019/ doi: 10.5194/amt-12-1393-2019